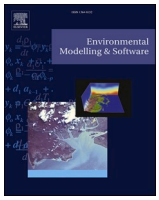
Environmental Modelling and Software 208 (2027) 107221



Contents lists available at ScienceDirect

Environmental Modelling and Software

journal homepage: www.elsevier.com/locate/envsoft



An integrated agent-based and hydrodynamic modelling framework for urban flood impact assessment using a risk priority index

Saeid Najjar-Ghabel [a], Farzad Piadeh [b], Kourosh Behzadian [a,*], Atiyeh Ardakanian [a]

[a] Smart Infrastructure and Green Technologies Research Group, School of Computing and Engineering, University of West London, St Mary's Rd, London, W5 5RF, UK
[b] Centre for Engineering Research, School of Physics, Engineering, Computer Science, University of Hertfordshire, Hatfield, AL10 9AB, UK

ARTICLE INFO

Keywords:
Agent-based modelling
Dynamic agent mapping
Demographic attributes
Hydrodynamic model
Road networks vulnerability

ABSTRACT

Agent-based models (ABMs) are widely used to investigate flood impacts on transportation systems, but many do not adequately represent behavioural adaptation and information diffusion. This study presents an integrated framework coupling a hydrodynamic flood model with an ABM to evaluate flood impacts on transport networks and road users in a part of the River Thames, London. A novel Risk Priority Index (RPI) was developed to quantify behavioural responses by integrating water depth, demographic vulnerability, and flood-warning information. Social information exchange among agents was simulated using a Watts-Strogatz small-world network. The hydrodynamic model was calibrated and validated using the Sequential Uncertainty Fitting (SUFI-2) approach, achieving R^2 values of 0.91 and 0.89, respectively. Results show that flooding disrupted approximately 9% of the road network, causing trip disruption rates of 51% on weekdays and 45% on weekends. The proposed framework supports the identification of vulnerable populations and critical roads for flood risk management.

Software and Data Availability

- **Name of software:** HEC-ABM
- **Developers:** Saeid Najjarghabel
- **Date first available:** July 2026
- **Software required:** Python 3.11, HEC-RAS 6.5
- **Program language:** Python
- **Source code:** https://github.com/Saeid-Najjarghabel/HEC-ABM.git
- **Documentation:** Workflow is provided in the repository README.
- **Input data:** OpenStreetMap road network, UK Environment Agency flow and water level observations, and UK Department for Transport traffic data.
- **Data availability:** Datasets used in this study are available in the GitHub repository.

1. Introduction

Floods rank among the most frequent and destructive natural disasters globally (Piadeh et al., 2022b, 2026). 3254 major flood events were recorded worldwide between 2000 and 2019, more than double the number recorded in the preceding two decades, causing substantial loss of life and economic and infrastructure damage (UNGA, 2016; Jonkman et al., 2024). The rising frequency and intensity of floods, attributed to climate change and urbanisation, underscore the necessity for enhanced flood risk mitigation strategies (Zhang et al., 2022; Bakhtiari et al., 2023). Urban environments are especially susceptible due to dense populations, intricate infrastructure networks, and socio-economic vulnerabilities (Bakhtiari et al., 2024). These factors reveal the shortcomings of conventional flood risk assessment approaches, which frequently overlook the complex interactions among flood dynamics, human behaviour, and mobility decisions (Jenkins et al., 2017; Lv et al., 2025).

* Corresponding author.
E-mail address: Kourosh.Behzadian@uwl.ac.uk (K. Behzadian).

https://doi.org/10.1016/j.envsoft.2026.107221
Received 4 July 2026; Received in revised form 27 October 2026; Accepted 30 October 2026
Available online 31 October 2026
1364-8152/© 2026 The Authors. Published by Elsevier Ltd. This is an open access article under the CC BY license (http://creativecommons.org/licenses/by/4.0/).

Conventional flood risk assessment has primarily relied on engineered protection measures and deterministic hydrological and hydraulic models to estimate flood hazards, including inundation extent and water depth (Piadeh et al., 2023). However, these methods frequently neglect human behaviour and social interactions, such as travel patterns, risk communication, and community responses, which substantially influence flood impact outcomes (Kunreuther and Pauly, 2006; Lo, 2013). Consequently, there is an increasing shift toward modelling frameworks that integrate both the physical dynamics of flooding and the behavioural responses of affected populations.

Between conventional depth-based hazard mapping and behavioural models, a further body of research has developed hazard indices specifically for people exposed to floodwater, combining water depth and flow velocity to assess pedestrian stability. These include empirically derived criteria based on depth and velocity (Cox et al., 2010) and mechanics-based, experimentally calibrated approaches, whose performance for extreme floods has been compared by Kvočka et al. (2016) and examined through the hydrodynamics of pedestrian instability by Arrighi et al. (2017). More recent work has combined depth and velocity into a single physics- and data-based impact parameter (Lazzarin et al., 2022) and mapped the loss probability of pedestrians to improve risk estimation and communication (Lazzarin et al., 2024). Compared with conventional hazard maps, these indices provide information more directly targeted to pedestrian safety. However, they describe the hazard at a location rather than how people's travel decisions and interactions change as a flood evolves.

Agent-based models (ABMs) have emerged to address this gap by effectively representing how individuals and groups make decisions under uncertain and hazardous conditions (Najjar Ghabel et al., 2019; Hamilton et al., 2020). These models employ a decentralised approach wherein agents interact with their environment and make decisions based on behavioural rules and contextual information (Crooks et al., 2021; Addai et al., 2025). Recent advances have integrated activity-based and agent-based modelling to incorporate mobility patterns, socio-economic factors, and hydrodynamic data, enabling simulation of daily activities during flood events (Lumbroso et al., 2023; Butters and Dawson, 2025). While activity-based models enhance behavioural realism by capturing travel motivations and timing (Auld and Mohammadian, 2012), they continue to face challenges in representing complex social interactions such as information sharing and group decision-making, which are essential for effective flood risk management (Templeton et al., 2024).

Table 1 summarises recent advances in integrating ABMs with hydraulic flood modelling frameworks, emphasising both methodological progress and existing conceptual gaps. Although two-dimensional (2D) hydraulic models have substantially enhanced the representation of

Table 1
Recent advances in agent-based flood risk assessment*.

Methodology	Physical model	Calibration Method (Hydraulic Part)	Agent-based model	Agent-agent interaction method	Highlights	Limitations	Reference
CLAIM	Physically based flood model (MIKE FLOOD)	Not reported	Individual and institutional ABM	Indirect agent-agent interactions	Explicit modelling of policies and institutions in flood risk management	High model complexity; intensive data requirements	Abebe et al. (2019)
ABMH and PMT	LISFLOOD-FP	Manual calibration of LISFLOOD-FP	A household- and government-based ABM	Not considered	Captures emergent levee and adaptation effects	Social interactions among households are implicit	Michaelis et al. (2020)
Coupled hydraulic-life-safety modelling framework	HEC-RAS 2D	Manually calibrated	Individual decision-making ABM	Indirect and infrastructure-mediated interactions	life loss and evacuation performance	Lack of peer-to-peer communication, or adaptive risk perception	El Bilali et al. (2021)
LSM for emergency planning	2D hydraulic models (e.g. HEC-RAS, TUFLOW)	Not reported	Multi-agent life-safety model	Group-based and word-of-mouth communication	Quantitative estimation of evacuation times and fatalities	Limited representation of social interaction and risk perception	Lumbroso et al. (2023)
Coupled flood-human dynamics modelling	SWMM	Not reported	Stakeholder-oriented multi-agent system	Indirect coordination through DCOP constraints	Explicit integration of stakeholder power and interest into decision-making	Lack of household-level behavioural adaptation	Nazemi et al. (2024)
CHANS framework	HiPIMS	Manual calibration using field and sensor data	Household-level ABM (FLAMEGPU)	Social links between households	High-resolution, real-time simulation of flood-human interaction	Social interactions are simplified and not explicitly network-based	Qin et al. (2024)
Integrated flood simulation with evacuation modelling	HEC-RAS 2D	Not reported	Resident- and authority-based ABM	Local neighbourhood interactions	Integrates machine learning to capture heterogeneous socio-demographic characteristics	Lacking explicit network structures or long-range information diffusion	Zhang et al. (2024)
Coupled hydrodynamic-ABM flood risk assessment	FloodArea and D8	Not reported	NetLogo-based ABM	Indirect interaction	Real-time, large-scale evacuation simulation	Lacking explicit peer-to-peer communication	Lv et al. (2025)

* The search is established based on the keywords such as “agent-based modelling”, “flood risk management”, and “urban flood modelling” in the Scopus search engine in title, abstract, and keywords for the last decade. Papers were reviewed, and relevant studies were selected.

Abbreviations:

- ABMH: Two-way coupled agent-based hydraulic modelling
- CLAIM: Coupled Flood-Agent-Institution Model
- CHANS: Coupled Human-Natural Systems
- D8: Flow routing algorithm
- DCOP: Distributed Constraint Optimisation
- FLAMEGPU: A graphical process unit simulator for domain-independent complex systems simulations
- FloodArea: Hydrodynamic model
- HEC-RAS 2D: Hydrologic Engineering Center's River Analysis System
- HiPIMS: High-Performance Integrated Hydrodynamic Modelling System
- LISFLOOD-FP: 2D hydraulic model
- LSM: Life Safety Model
- NetLogo: Platform for agent-based modelling
- PMT: Protection Motivation Theory
- SWMM: Storm Water Management Model

physical flood dynamics within coupled frameworks, the modelling of social processes such as information exchange and interpersonal interactions among agents remains underdeveloped. Several studies incorporate behavioural responses through institutional structures or governance frameworks instead of direct agent-to-agent interactions (Abebe et al., 2019; Michaelis et al., 2020). Models focused on life safety typically prioritise evacuation efficiency and fatality estimation, where interactions occur mainly through shared infrastructure, group movement, or limited word-of-mouth communication (El Bilali et al., 2021; Lumbroso et al., 2023). Recent decentralised and high-performance frameworks exhibit similar limitations. For instance, a stakeholder decision-making has been modelled using distributed optimisation approaches that abstract interactions into system constraints rather than behavioural adaptation (Nazemi et al., 2024). Additionally, large-scale coupled human-natural system models represent social dynamics through simplified behavioural rules rather than explicit social networks (Qin et al., 2024). Behaviourally oriented evacuation studies include opinion dynamics and machine-learning-based heterogeneity; however, interactions are generally confined to local or proximity-based exchanges without long-range information diffusion (Zhang et al., 2024). Likewise, real-time evacuation simulations under dynamic flood conditions predominantly rely on transport-system interactions and congestion dynamics instead of peer-to-peer communication (Lv et al., 2025). These studies highlight that despite substantial advances in coupling ABMs with hydraulic models, explicit, network-driven social interactions and dynamic risk behaviour in agent-based modelling remain under-represented.

Significantly, these investigations exhibit varied calibration approaches for hydraulic elements, ranging from manual adjustment to sensitivity evaluations (Michaelis et al., 2020; Qin et al., 2024). A critical observation is that few approaches systematically address parameter uncertainty, even though it plays a central role in determining the robustness of flood predictions. Only a limited number of studies explicitly quantify the effects of parameter uncertainty on predicted inundation dynamics and associated human impacts. In contrast, uncertainty-based calibration frameworks, such as the sequential uncertainty fitting algorithm (SUFI-2), offer a more rigorous solution. SUFI-2 have been extensively applied to calibrate hydrodynamic models (Masoumi et al., 2020, 2021). These model types can simultaneously calibrate and assess model uncertainty, delivering accurate and reliable models.

Based on the above-mentioned studies, the explicit representation of information dissemination and risk communication within integrated flood modelling frameworks remains limited. Furthermore, many previous agent-based flood models also rely on simplified behavioural assumptions, reducing their ability to realistically represent behavioural adaptation processes. In addition, the reliability of coupled flood-behaviour simulations strongly depends on the accuracy of the underlying hydrodynamic model. Uncertainty-based calibration approaches are essential for improving the robustness of flood depth and inundation predictions by accounting for uncertainties in model parameters.

This study proposes an integrated flood inundation modelling framework that combines a hydrodynamic model with a dynamic, risk-aware agent-based model to address limitations in existing flood risk assessments. The framework incorporates uncertainty-based hydrodynamic calibration and links the resulting flood simulations to a risk-based agent-based model that represents urban populations, daily mobility patterns, and behavioural responses. Flood exposure, demographic vulnerability, institutional communication, and transportation dynamics are integrated through a risk index to evaluate flood impacts on both people and road networks. In addition, a social network modelling approach based on information sharing among agents is implemented to simulate the social influence, and behavioural adaptation during flood events. The framework further integrates dynamic road closures, traffic congestion, and agent interactions to provide a more realistic representation of urban flood disruption. This approach enables a more comprehensive assessment of urban flood risk by jointly capturing physical flood processes and evolving human responses.

2. Methodology

Fig. 1 presents the proposed integrated framework for adaptive flood risk assessment, linking hydrodynamic modelling with an ABM through four primary steps. The process starts by integrating three types of input data, including flood modelling data, social behaviour data, and spatial datasets, to support both physical flood simulation and behavioural modelling components. Subsequently, a 2D flood simulation is developed in HEC-RAS, with defined boundary conditions and the generation of flood depth and inundation maps. The hydraulic model is calibrated using the SUFI-2 algorithm to optimise parameters and quantify uncertainty.

The subsequent step involves developing the ABM, which integrates stakeholder analysis and introduces a dynamic behavioural risk metric (RPI). This index combines flood depth, demographic attributes, and institutional communication, while social information diffusion is modelled using a Watts-Strogatz network. An activity-based mobility model grounded in the ADAPTS framework, which is the dynamic activity planning and travel scheduling model, introduced by Auld and Mohammadian (2012), simulates daily travel behaviour, supported by A* pathfinding and the Nagel-Schreckenberg traffic model. Finally, the hydrodynamic and ABM components are integrated to evaluate flood impacts using threshold-based criteria for flood depth and RPI, facilitating adaptive impact mapping and evaluation of road network performance and population vulnerability. Detailed descriptions of each modelling component are provided in the following subsections.

2.1. Data collection and acquisition

The data collection process was organised into three main categories, including flood modelling data, social behaviour data, and spatial datasets. Flood modelling data included the hydrological, hydraulic, and terrain information required for the 2D hydrodynamic simulations, such as river geometry and boundary conditions from the Environment Agency (EA) (Environment Agency, 2025). A high-resolution terrain dataset derived from LiDAR data (light detection and ranging) provided by the EA was also utilised. This dataset combines a 1 m resolution DTM (digital terrain model) representing the floodplain surface and a 0.5 m resolution bathymetric dataset representing the riverbed geometry of the River Thames. Moreover, Land-cover data with a spatial resolution of 10m × 10m from the UK Centre for Ecology & Hydrology (2025) were employed in the hydrodynamic model to parameterise surface roughness. Social and travel behaviour data from the London Travel Demand Survey (LTDS) (Transport for London, 2024) were used to represent population characteristics, daily mobility patterns, and behavioural heterogeneity within the agent-based model.

Additionally, spatial datasets, including building locations and population distribution data from the 2021 UK Census provided by the Office for National Statistics (Office for National Statistics, 2021), along with the road network from OpenStreetMap (OpenStreetMap, 2025) were used to represent the physical environment and support routing and traffic simulation. All datasets were harmonised to a common coordinate reference system and spatial resolution to ensure compatibility between the hydrodynamic model and the agent-based simulation.

2.2. Hydrodynamic model

2.2.1. Model setup

Flood dynamics were simulated using a 2D hydrodynamic model implemented in HEC-RAS. The model incorporated river geometry, floodplain topography derived from high-resolution DTM data, and boundary conditions including, upstream discharge hydrographs from EA gauging records and a downstream friction slope. A hybrid

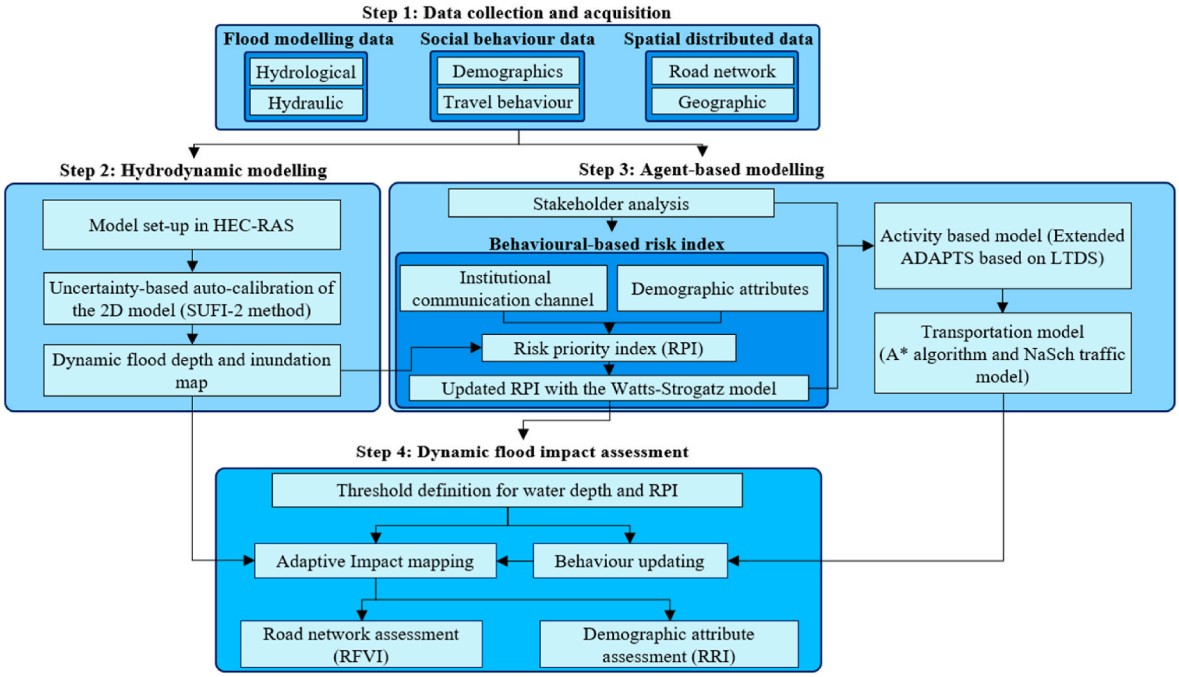


Fig. 1. Workflow of the proposed method for dynamic flood risk assessment using coupled agent-based and hydrodynamic models.

computational mesh combining structured and unstructured cells was employed to enhance spatial resolution in critical areas such as riverbanks and urban flood zones. The hydrodynamic model was dynamically coupled with the ABM through a controller that managed data exchange at 30-min intervals. HEC-RAS generates spatial water-depth maps exported as raster layers, which were subsequently read by the ABM to update agent behaviour under evolving flood conditions.

2.2.2. *Uncertainty-based auto-calibration of the 2D hydrodynamic model*

Calibration primarily focused on spatially distributed hydraulic roughness by adjusting Manning's *n* values associated with different land-cover classes, while the channel geometry, computational mesh, and boundary conditions were kept fixed during the calibration process. The calibration was performed using the Sequential uncertainty fitting algorithm (SUFI-2), an uncertainty-based optimisation approach widely used for hydrological and hydrodynamic model calibration. SUFI-2 simultaneously accounts for parameter uncertainty and model prediction uncertainty by iteratively adjusting parameter ranges to maximise the agreement between simulated and observed data while ensuring that most observations fall within the 95% prediction uncertainty (95PPU) band.

The calibration performance was evaluated using the coefficient of determination (R^2), and two other factors were employed to quantify prediction uncertainty via the 95PPU band: the *p-factor*, representing the fraction of observations enclosed within the uncertainty band, and the *d-factor* representing the mean bandwidth normalised by the standard deviation of the observations. The *d-factor* is calculated by Equation (2), where $\bar{d}_x$ represents the mean of the upper and lower limits of the 95PPU band, calculated by Equation (1) as follows:

$$\bar{d}_x = \frac{1}{k}\sum_{z=1}^{k}\left(X_{U,z} - X_{L,z}\right) \tag{1}$$

$$d-factor = \frac{\bar{d}_x}{\sigma_x} \tag{2}$$

In these equations, σ_x represents the standard deviation of the observations, for each time step z, $X_{U,z}$ and $X_{L,z}$ are the 97.5th and 2.5th percentiles from the Latin Hypercube (*LH*) ensemble (Solomatine and Ostfeld, 2008), respectively, while k represents the number of observations. SUFI-2 samples parameters using a uniform *LH* distribution. By design, better calibration is indicated by a larger *p-factor* and a smaller *d-factor*. In practice, with this algorithm, both metrics may initially exhibit relatively large values during the early iterations and gradually stabilise. Further details on the basic formulations of the SUFI-2 algorithm are provided in Appendix A.

To evaluate how hydraulic parameter uncertainty propagates into the impact metrics, the 18 behavioural parameter sets ($R^2 \geq 0.80$) from the SUFI-2 calibration were also used to simulate the 100-year event, and each resulting depth field was used to drive the coupled HEC-RAS-ABM simulation (Section 3.4.1).

2.3. *Agent-based model*

2.3.1. *Stakeholder analysis*

This study classifies agents into two primary categories: EA and community members, as they are considered the key stakeholders in flood risk management (Piadeh et al., 2022a; Bakhtiari et al., 2024). The EA plays a vital role in flood risk monitoring, issuing warnings, and coordinating response actions. Its behaviour is dynamic, as it continuously updates flood forecasts and disseminates emergency guidance. Community members, including pedestrians and vehicle users, exhibit adaptive behaviours in response to flood warnings, traffic conditions, and social influences. Their mobility patterns evolve in response to risk priority, environmental constraints, and the progression of flood events. Moreover, their associated vulnerability factors are determined by demographic variables such as age and employment status. Furthermore, infrastructure elements, including roads, educational buildings, residential areas, commercial properties, and recreational centres are represented as the origin or destination points within the ABM.

2.3.2. *Behaviour-based risk index and social interaction model*

A dynamic risk index (RPI) was incorporated to explicitly represent agents perceived external threat and enable adaptive, threshold-driven decision-making under flood conditions. The RPI integrates physical flood exposure, institutional communication channels, and de-

mographic vulnerability into a single bounded index that directly governs agents' mobility and activity choices. The RPI for agent i at time t is defined as Equation (3):

$$RPI_i(t) = \min\left(1, \max\left(0, (\alpha \times f(D_i(t)) + \beta \times C(t)) \times M_i\right)\right) \quad (3)$$

Where $f(D_i(t))$ represents the nonlinear perception of local floodwater depth by agent i at time step t, modelled using a sigmoid function using Equation (4) to capture threshold-based human responses to increasing water levels. This allows small water depths to be largely ignored, while rapidly escalating perceived risk once a tolerance threshold is exceeded. The official warning level, $C(t)$, is derived from the simulated water level at the observation point, consistent with the thresholds used by the EA. The warning level is defined as Equation (5). The parameters α and β control the relative influence of direct environmental exposure and institutional information, respectively. The weights were set to $\alpha = 0.7$ and $\beta = 0.3$, giving greater weight to directly experienced flood conditions than to area-wide warnings (these parameters were also analysed in section 3.4.3).

$$f(D_i(t)) = \frac{1}{1 + e^{-k(D_i(t) - T)}} \quad (4)$$

Where, $D_i(t)$ represents the local water depth at the agent's location, and T and k are the water depth threshold and sensitivity slope, respectively. The depth-disruption function governing vehicle speed (Pregnolato et al., 2017) and the depth-based loss-of-stability function governing pedestrian danger (Lazzarin et al., 2022, 2024) are nonlinear and threshold-concentrated curves. Using the same functional family for the behavioural response keeps the model internally consistent rather than pairing a linear perception term with nonlinear physical hazard terms. The threshold T was set to 0.30 m, consistent with the depth at which vehicle movement becomes impractical (Pregnolato et al., 2017), and the slope was set to k = 10 m^{-1}, which corresponds closely to the steepness of the loss-probability function for pedestrians proposed by Lazzarin et al. (2024).

$$C(t) = \begin{cases} 0, & H_t < 5.15 \\ 0.5, & 5.15 \le H_t < 5.77 \\ 1, & H_t \ge 5.77 \end{cases} \quad (5)$$

Where, H_t denotes the water level at the Kingston Station at the time t. Based on the EA data, the flood alert threshold for low-lying land flooding, and the level above which property flooding becomes possible are 5.15 and 5.77, respectively. $C(t)$ represents the level of official flood warning available to agents at time t and can be different based on the level of warning, with 0 (no warning), 0.5 (alert-level warning), and 1 (severe-level warning). In the present case study, $C(t)$ was derived from the water level at Kingston Station and the EA warning thresholds for this station (Eq. (5)). In other applications, the warning levels and their numerical values should be defined according to the local warning system.

Agent heterogeneity is incorporated through the demographic modifier, M_i, which acts as a vulnerability-based amplification factor shown in Equation (6):

$$M_i = 1 + (AgeFactor_i + EmploymentFactor_i) \quad (6)$$

This modifier captures how different population groups are affected under the same flood condition. Agents in vulnerable age groups (i.e., children and seniors) or those experiencing financial insecurity (i.e., unemployed agents) have a higher vulnerability. As a result, two agents exposed to the same flood conditions may exhibit different behavioural responses, reflecting realistic social and demographic diversity. For the vulnerable age groups, an additional value of 0.1 was assigned to reflect increased physical vulnerability during flood events. Similarly, agents who were unemployed were assigned an additional value of 0.1 (i.e., $EmploymentFactor = 0.1$) to represent heightened sensitivity to potential economic and safety-related losses.

The RPI functions as an active decision trigger rather than a passive perception score. Higher RPI values indicate that the external environment is perceived as increasingly unsafe, increasing the likelihood of behavioural adaptation such as cancelling trips and remaining at home. Conversely, lower RPI values correspond to delayed reactions or to continued normal activity.

Flow velocity was not included in the RPI primarily because the study area is a lowland reach of the River Thames subject to slow-rising fluvial flooding, where floodplain velocities are generally low. Under these conditions, water depth is the dominant hazard variable. Moreover, the RPI governs travel decisions, and both official flood communication and people's perception of flood severity are mainly depth-based. EA warnings are issued on water-level thresholds, and water depth on a road is the most visible cue for road users. Also, road closure, which drives the network-disruption results, follows vehicle-related depth criteria; the depth-disruption function of Pregnolato et al. (2017). Nevertheless, several studies have shown that flow velocity strongly affects the stability of people in floodwater (Cox et al., 2010; Kvočka et al., 2016; Arrighi et al., 2017; Lazzarin et al., 2022, 2024). The depth-only formulation may therefore underestimate the hazard to pedestrians and cyclists in locations where the flow is faster, such as bridge approaches, riverbanks and areas close to the main channel.

Moreover, social networks play a critical role in influencing agents' behaviour, information dissemination, and decision-making during flood events. In an ABM, social networks can be explicitly modelled to simulate how individuals interact, share risk information, and influence each other's decisions (Templeton et al., 2024). Here, we employed the risk-priority evolution method to account for the dynamic adjustment of social influence during flood events. Therefore, the RPI is not static and evolves based on social discussions, and is defined as Equation (7):

$$RPI_i(t+1) = \lambda * RPI_i(t) + (1-\lambda)\sum_{j \epsilon S_i} W_{ij} RPI_j(t) \quad (7)$$

Where, $RPI_i(t)$ and $RPI_j(t)$ are the risk-priority indices of agents i and j at time t. λ represents the social-influence factor (higher λ means others have less influence on the agent). Here we assumed a balanced condition (i.e., $\lambda = 0.5$) based on the sensitivity analysis (results are in Section 3.4.1). S_i denotes the set of social neighbours of agent i (which is calculated using the Watts-Strogatz model) and W_{ij} is the normalised influence of neighbour j on agent i, and here, equal social weights are assigned to each neighbour (i.e., $W_{ij} = 1/|S_i|$).

The Watts-Strogatz model was used to compute the social neighbours, and the RPIs of those neighbours were then averaged for each agent. This model is a graph generation algorithm designed to replicate the small-world properties observed in many real-world social, biological, and technological networks (Watts and Strogatz, 1998). In the context of agent-based modelling, especially during flood events, it serves as a realistic approximation of social networks, capturing both local clustering (friends and neighbours) and long-range connections (social media or distant acquaintances). In this study, each agent communicates with its neighbours in the network to share flood-risk information and to influence each other's RPI.

2.3.3. Risk-based activity model

In this study, the extended ADAPTS model with RPI represents the daily travel decisions and scheduling behaviours of urban residents. ADAPTS enables more realistic, adaptive modelling of flood-induced disruptions, as individuals dynamically adjust their travel plans in response to flooding (Zhuo and Han, 2020). This model is particularly strong at capturing dynamic, context-sensitive decisions across individuals' daily routines, making it well-suited for integration with agent-based models in complex urban systems (Shabanpour et al., 2018; Auld and Mohammadian, 2012).

The extended ADAPTS workflow is summarised in Fig. 2, showing how each agent progresses through activity generation, trip planning,

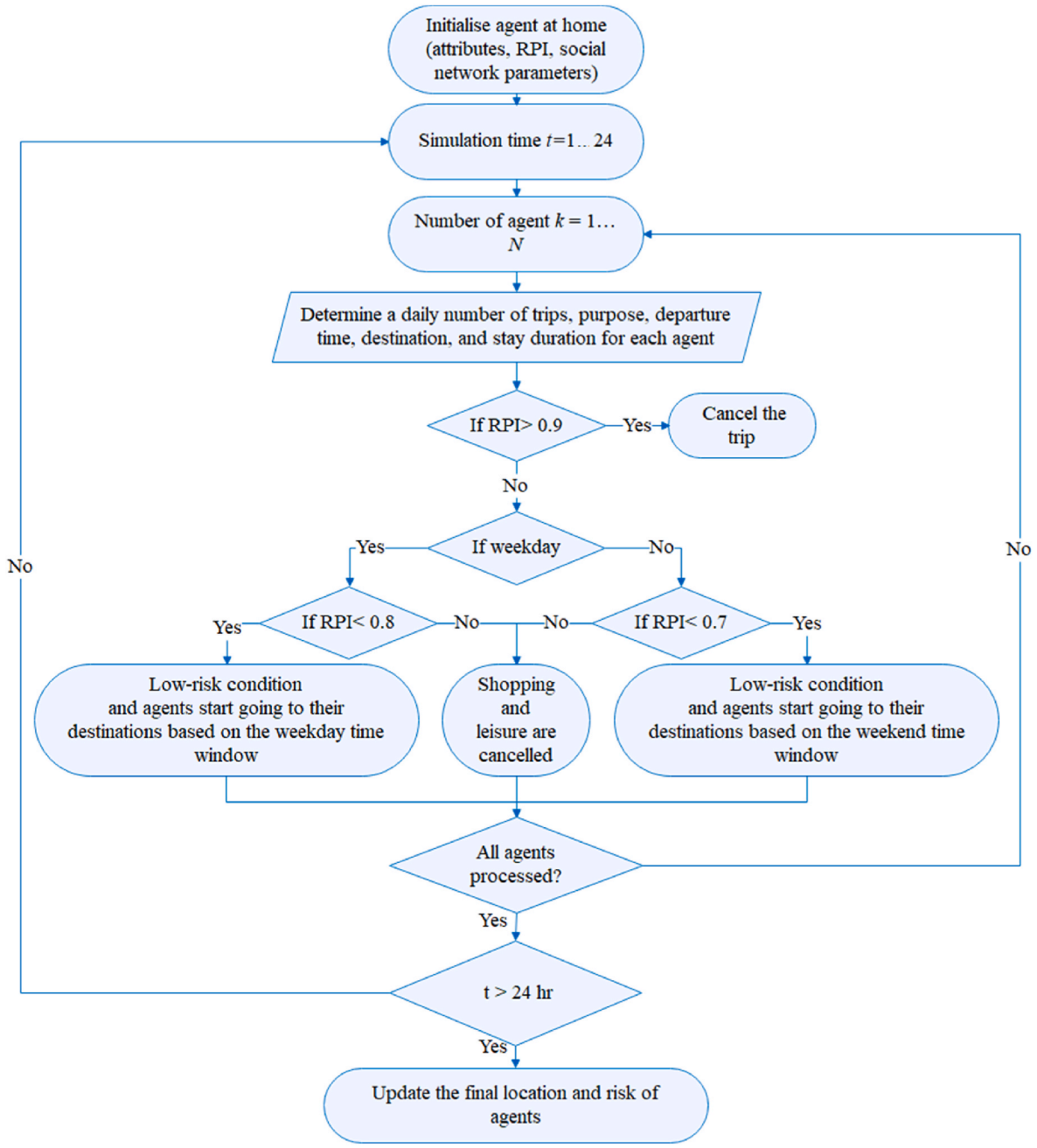


Fig. 2. Daily activity model for each agent.

and execution. Agents begin their day at home, drafting a daily activity schedule based on the trip's purpose, duration, destination, and departure time. Activity execution is then conditioned on the agent's RPI through two cancellation thresholds (θ), which depend on the purpose of the trip. Commuting trips (to work or to education) are essential and difficult to postpone, so they are cancelled only when the perceived risk is very high (RPI > 0.9). Discretionary trips (shopping, leisure and other personal trips) can be postponed more easily and are therefore cancelled at a lower level of perceived risk (RPI > 0.8 on weekdays and RPI > 0.7 on weekends). As a flood develops, an agent thus first gives up its discretionary trips and, if its RPI continues to rise, also its commuting trips, remaining at home. Agents proceed with their scheduled activities in the low-risk conditions, following weekday- or weekend-specific departure windows. This decision logic ensures that travel behaviour dynamically responds to evolving flood conditions.

The model incorporates detailed behavioural patterns derived from the LTDS to generate realistic daily mobility schedules that capture distinct weekday-weekend differences in travel demand (Fig. 3). On weekdays, travel activity is more intensive in the morning and evening, dominated by work and educational trips. In contrast, weekends exhibit reduced mandatory travel and increased shopping and leisure-related trips concentrated between 11:00 and 16:00. These LTDS-derived heatmaps are operationalised through weighted departure-time distributions, whereby each agent draws a Poisson-distributed number of trips, selects a trip purpose, and samples a departure time from the corresponding weekday or weekend probability distribution.

2.3.4. *Transportation model*

Road networks were extracted from OpenStreetMap (OSM), and routing was performed using the A* algorithm (Hart et al., 1968; Dechter and Pearl, 1985) inspired by the Google Maps API, to compute agent routes and traffic delays. Traffic dynamics were simulated using

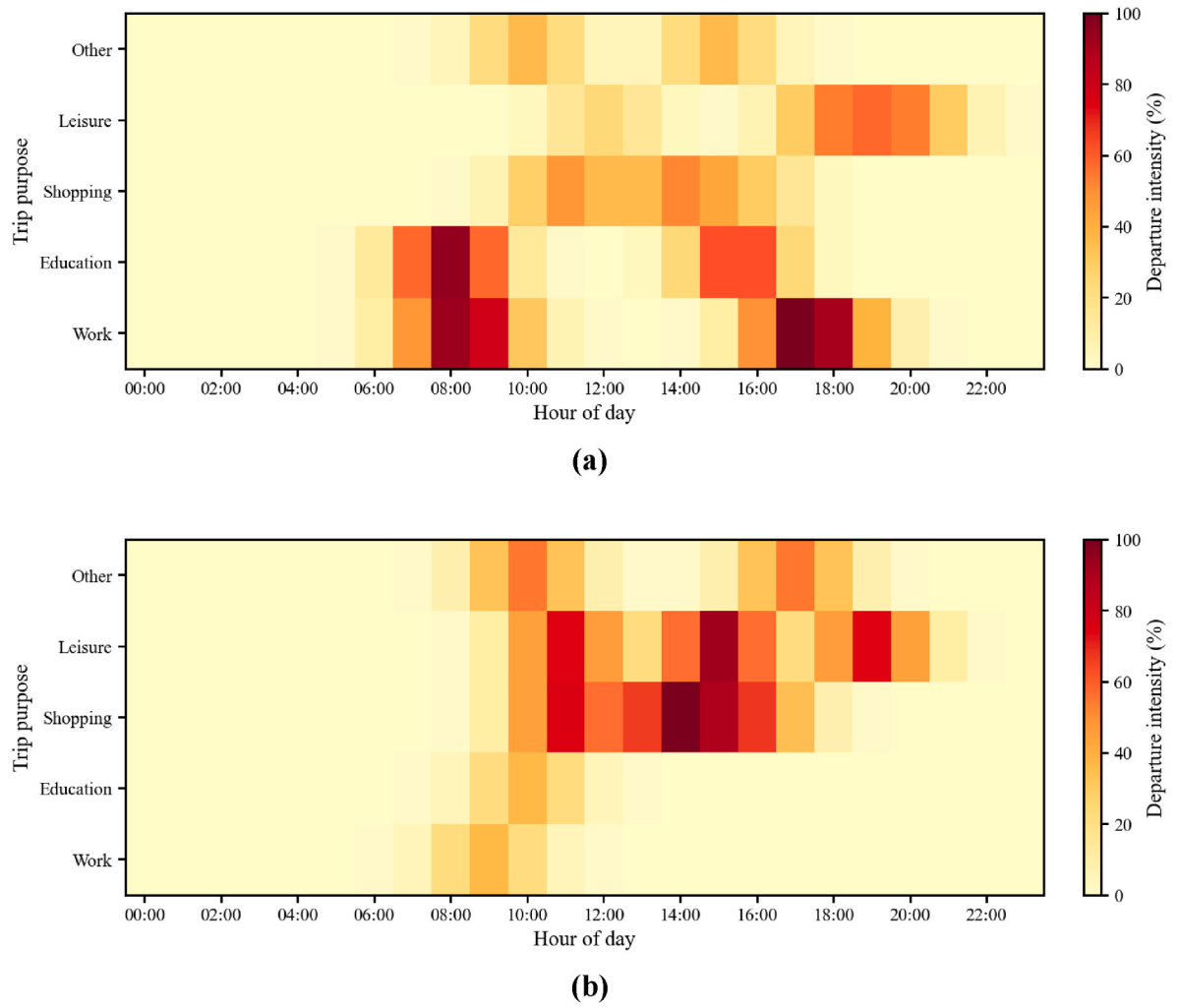


Fig. 3. Departure intensity for different activities of the residents at (a) weekday and (b) weekend (based on the LTDS data, Transport for London, 2024).

the Nagel-Schreckenberg (NaSch) cellular-automaton model (Nagel et al., 1998), allowing congestion to emerge dynamically during the simulation.

The A* algorithm calculates optimal routes by minimising travel cost based on actual and estimated distances, while the NaSch cellular automaton captures traffic flow and vehicle interactions by updating vehicle speed and position according to acceleration, braking, randomisation, and movement rules. Agents travel by walking, cycling, driving, or public transport, with base speeds of 4, 12, 25, and 20 km/h, respectively and their speeds are dynamically adjusted using congestion factors from the NaSch model.

In this framework, the NaSch model is used as a road-segment-level traffic dynamics module rather than a direct representation of each ABM agent as an individual vehicle. For each road segment, traffic density is converted into a number of simulated vehicles distributed across discrete cells. The NaSch update rules are then applied to estimate the average traffic speed on that segment. The resulting traffic factor is subsequently used to adjust agent travel speeds within the ABM.

2.4. Impact of flood on road networks and demographic attributes

In this study, flood risk is understood as the combination of hazard, exposure and vulnerability, and each component of the framework is linked to a specific model variable. The hazard is the flood condition that can cause adverse consequences, represented by the time-varying water depth simulated by HEC-RAS. Exposure is the presence of people or road segments where the hazard exceeds a critical threshold at a given time. An agent is considered exposed when the water depth at its location exceeds 0.30 m while it is engaged in the travel cycle, and a road segment is closed when the depth on it exceeds the same threshold. The relative risk index (RRI, Equation (11)) summarises exposure at group level, as the likelihood that members of a demographic group are exposed relative to the average active agent. Vulnerability refers to characteristics that increase susceptibility to adverse consequences under the same hazard. For people, it is represented by the demographic modifier M_i (Equation (6)). For roads, it is represented by the near-threshold component of the road flood vulnerability index (C_{near}, Equation (9)), which describes how often a segment remains close to becoming impassable. The behavioural response of agents is governed by the risk priority index (RPI, Equations (3)–(7)), which expresses perceived threat and priority in travel decisions rather than risk itself. Finally, the impact of flooding is measured by the resulting disruption to mobility and the network, namely failed trips, closed roads and the number of travelling agents. The term "relative risk" in the RRI is used in its epidemiological sense, as the ratio between the rate of an outcome in a group and the rate in a reference population; it does not denote risk as the combination of hazard, exposure and vulnerability.

Dynamic road closures are implemented to represent flood-induced infrastructure disruption based on simulated water depth at each time step. For every road segment, a set of sample points along the road geometry is evaluated in the flood model, and a segment is considered closed (and temporarily removed from the routing graph) when the

flood depth at any sampled point exceeds the closure threshold of 0.30 m, consistent with the depth-disruption function of (Pregnolato et al., 2017), derived from experimental, observational and video data. When road closures occur, agents dynamically recalculate alternative routes to their destinations using the A* pathfinding algorithm, allowing them to interact with and adapt to evolving flood conditions through route modification, congestion redistribution, and changes in travel behaviour during the simulation.

The impact of flooding on the road network is assessed by tracking the spatial and temporal distribution of closed road segments by evaluating the road flood vulnerability index (RFVI), Equation (10), which captures not only flood exceedance frequency calculated using Equation (8) but also the threshold sensitivity of flooding for each road link calculated by Equation (9).

$$C_{exceed} = \frac{1}{T}\sum_{t=1}^{T} I(d_e(t) \geq D_c) \tag{8}$$

$$C_{near} = \frac{1}{T}\sum_{t=1}^{T} I(\ |d_e(t) - D_c| \leq \Delta) \tag{9}$$

$$RFVI_e = w_{exceed}C_{exceed} + w_{near}C_{near} \tag{10}$$

Where C_{exceed} represents the exceedance frequency, defined as the proportion of simulation time steps (T) during which the flood depth on the road segment e, denoted by $d_e(t)$, exceeds the critical closure threshold, D_c. The indicator function I returns 1 when the condition is satisfied and 0 otherwise. Equation (9) defines C_{near}, which measures the near-threshold frequency, indicating how often the flood depth remains within a tolerance band Δ around the closure threshold, thereby capturing situations where the road is close to becoming impassable.

In parallel, the model evaluates individual-level consequences by tracking agent status and travel outcomes at each simulation time step. Agents are classified into three statuses. Travelling agents represent the active-mobility population and include all agents engaged in the travel cycle, encompassing physical movement along the transport network as well as the pre-departure and activity-duration phases associated with an ongoing trip chain. These agents are therefore considered dynamically exposed to flood-induced transport disruption throughout their mobility process. Failed-trip agents represent individuals who intend to travel but are unable to initiate or complete a trip due to network disconnection or the absence of a feasible route under flooded conditions. Finally, Idle agents denote individuals who are not engaged in the travel cycle and have no active or imminent travel demand, typically remaining at fixed locations such as their home.

Additionally, demographic attributes, including age group, employment-status group, and travel-mode group, are analysed to assess differential exposure and behavioural response to transport disruption across population groups. A relative risk index (RRI) is computed by Equation (11) to quantify exposure on a per-capita basis. For each demographic group, g, at time step t, the RRI is defined as the ratio between the group-specific exposure rate and the overall population exposure rate:

$$RRI_{g,t} = \frac{NE_{g,t}/NP_g}{NE_t/N_t} \tag{11}$$

Where $NE_{g,t}$ denotes the number of exposed individuals in the group g, at the time t, NP_g is the total population of the group g, NE_t, is the total number of exposed individuals at time t, and N_t is the total simulated population. An RRI value greater than 1 indicates that a group experiences higher-than-average exposure relative to its population share, while values below 1 indicate comparatively lower likelihood of exposure. This index helps identify when and which demographic groups are most affected during peak-inundation and network-disruption phases.

3. Result and discussion

3.1. Case study

The study area selected for this research is located along part of the River Thames, located in the Thames Catchment, downstream of the Maidenhead-to-Sunbury sub-catchment (Fig. 4). The study area comprises a heterogeneous landscape consisting of broadleaved woodland, improved grassland, urban and suburban areas, and freshwater bodies. In the calibration of the hydrodynamic model, the land-cover map shown in Fig. 4 was used to spatially assign Manning's roughness coefficients (n) across the model domain.

The spatial distribution of people, buildings and the main road network is shown in Fig. 5. The case study population is grouped, and each dot in Fig. 5a represents 200 individuals (similar to Khoshkonesh et al., 2024), highlighting densely populated areas that require targeted flood management planning. It should be noted that the term agent in this study refers to groups of individuals, and all demographic attributes are assigned at the group level. Agents are randomly distributed across the study area based on the population-density map derived from the 2021 census data (Office for National Statistics, 2021).

The case-study population is aggregated so that each agent represents 200 individuals (similar to Khoshkonesh et al., 2024). This aggregation was adopted to keep the computational cost of dynamic routing and repeated ensemble simulations manageable; the framework itself can be applied at the level of individual persons or households. Because demographic attributes are assigned at group level, heterogeneity within each group is not represented, exposure changes in discrete steps, and social links represent exchanges between groups. A test for the whole study area with 100 and 50 individuals per agent (Appendix B; Figure B1) changed peak failed trips by less than 1 percentage point (Figure B2).

The proportional distribution of agent attributes used in the model, including age groups, employment status, and travel-mode preferences for weekdays and weekends, is presented in Table 2. Age is classified into three groups: children, adults, and seniors. Employment status is represented by three groups: employed, unemployed, and students. Travel-mode preferences also vary according to the day type. For weekdays, agents travel as walkers, cyclists, public transport passengers (PTP), or drivers. In contrast, weekend travel patterns show slightly different proportions. The demographic and behavioural attributes assigned to the agents were generated using distributions derived from the 2021 census data (Office for National Statistics, 2021) to ensure that the simulated population reflects realistic travel behaviour in the study area.

Fig. 6 presents designed hydrographs at Kingston Station for the 100-year flood. The flood-threshold level at this station is 5.15 m, as reported by the EA and indicated by the dashed red line in this figure. The hydrograph exhibits a distinct peak flow, reaching approximately 786 m^3/s for the 100-year flood. This hydrograph was used as the upstream boundary condition in the hydrodynamic model and the resulting flood simulations were subsequently linked to the agent-based model.

3.2. Preliminary results on calibration and validation of the hydrodynamic model

The HEC-RAS hydrodynamic model was calibrated and validated against multiple historical flood events at Kingston Station using the SUFI-2 algorithm to optimise Manning's n values across different land-cover classes, ensuring accurate and reliable flood-dynamics simulations. Each land-cover class was assigned an initial Manning's coefficient (n) in the calibration process (Table 3), with defined upper and lower bounds representing physically realistic ranges. The SUFI-2 algorithm iteratively adjusted these parameters to minimise *d-factor* and maximise *p-factor*. The final best-fit values are consistent with field conditions,

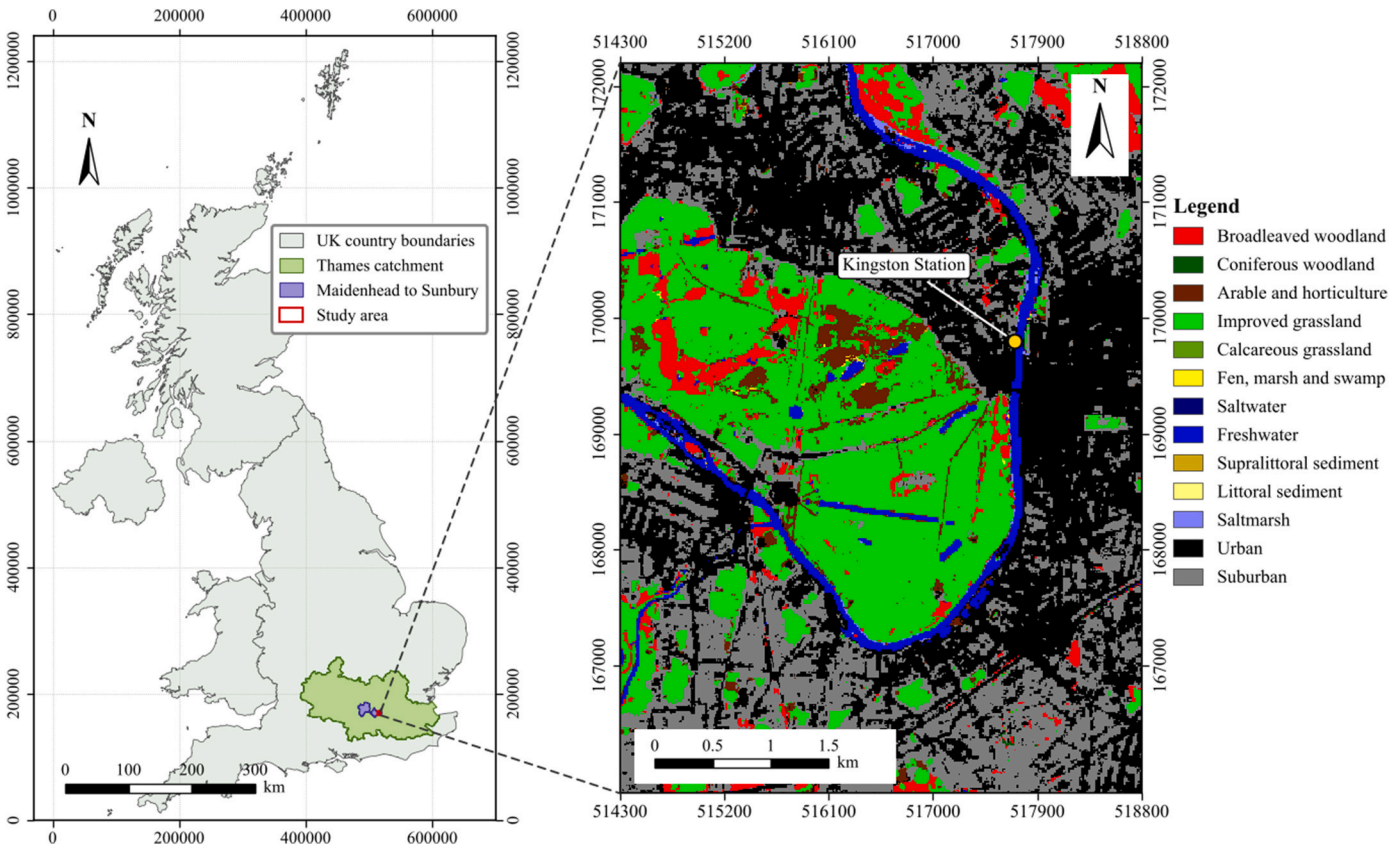


Fig. 4. The River Thames from Maidenhead to Sunbury, and the land cover map of Kingston upon Thames.

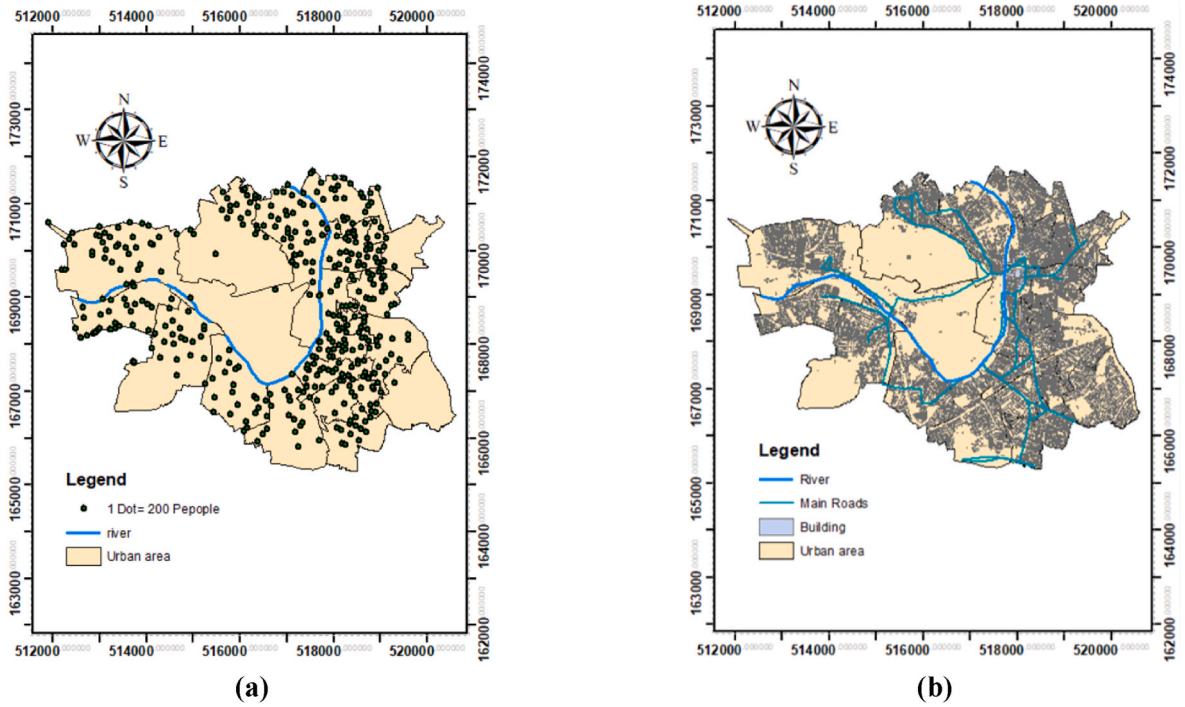


Fig. 5. Spatial distribution of (a) people, and (b) buildings and main road network.

with higher n values for densely vegetated areas (e.g., Coniferous Woodland, $n = 0.101$) and lower n values for smooth surfaces such as Supralittoral and Littoral Sediment ($n = 0.018$).

Fig. 7 compares observed and simulated discharges for the 2020 and 2024 flood events. The 2020 flood event showed a rapid rise in flow up to 435 m^3/s, followed by a short-duration peak and gradual decline, while the 2024 event exhibited a lower but more sustained peak of about 414 m^3/s. The 2020 and 2024 flood events were used to calibrate and

Table 2
Attributes of agents (Office for National Statistics, 2021).

Attribute Category	Time Window	Type	Percentage
Age	-	Children	20%
		Adults	62%
		Seniors	18%
Employment status	-	Employed	65%
		Unemployed	10%
		Student	25%
Travel mode	Weekday	Walkers	27%
		Cyclists	10%
		PTP	25%
		Drivers	38%
	Weekend	Walkers	35%
		Cyclists	8%
		PTP	27%
		Drivers	30%

validate the hydrodynamic model, respectively. The 2020 calibration (Fig. 7a) achieved good agreement with observations, achieving an R^2 value of 0.91. The *p-factor* = 0.809 indicates that 80.9% of the observed data fell within the 95PPU band. Also, the *d-factor* = 0.768 demonstrates that the uncertainty-band width was well-proportioned relative to the observed variability.

Validation against the 2024 flood event (Fig. 7b) produced an R^2 value of 0.89. The close agreement between the observed and simulated discharge indicates that the model reproduces both the timing and magnitude of the peak flow at Kingston Station, and that the calibrated parameters are transferable to an independent event of similar magnitude. However, agreement at a single gauging station does not by itself demonstrate that local water depths are reproduced across the floodplain.

The performance of the hydrodynamic model was also evaluated against the Flood Risk Zone 2 provided by the EA and FastFlood platform for the 100-year flood. In the UK, Flood Zone 2 signifies a medium flood risk (0.1-1% annual chance from rivers, 0.1-0.5% from sea), requiring a flood risk assessment for development. Figure C in Appendix C compares the flood-inundation map generated by the HEC-RAS model, EA, and the FastFlood platform.

3.3. Flood impact assessment on the road networks and population groups

The RFVI map is shown in Fig. 8 under the maximum water depth of the 100-year flood scenario. This figure shows a clear spatial concentration of road vulnerability along the Thames corridor and key bridges, with the highest criticality observed on Hampton Court Road bridge and Sopwith Way, with RFVI values of 0.69 and 0.57, respectively. High vulnerability is also evident along Horse Fair (RFVI = 0.56) and Wheatfield Way (RFVI = 0.51), reflecting their proximity to inundated zones and their functional importance in maintaining cross-river and corridor connectivity. In contrast, routes such as Portsmouth Road, Riverbank, Kingston Road, and Creek Road connectors exhibit comparatively lower average vulnerability, with an average RFVI of approximately 0.45. These findings provide a clear basis for targeted flood-risk management interventions, suggesting that authorities should prioritise strengthening and upgrading riverbank flood defence systems adjacent to these critical corridors to reduce inundation depth, minimise closure risk, and enhance overall transport network resilience.

The weekday and weekend spatial results (Fig. 9) illustrate how flood propagation along the River Thames corridor progressively disrupts the transport network and affects agent mobility patterns. In both the weekday and weekend scenarios, flooding initially impacts riverside corridors and bridge approaches in the late morning and expands significantly by the evening, resulting in an increased number of flooded road segments and network fragmentation. As inundation intensifies, clusters of failed trips emerge near disconnected road links and bridge access points, while the number of travelling agents decreases in these areas due to the loss of feasible routes. However, the disruption is more significant in the weekday scenario (Fig. 9a and b), where higher commuting demand leads to denser clusters of failed trips and greater mobility disruption around critical corridors, whereas weekend patterns

Table 3
Manning's values used in the SUFI-2 calibration process for different land cover classes.

Land cover class	Initial value	Lower bound	Upper bound	Best value (SUFI-2)
Broadleaved Woodland	0.070	0.055	0.110	0.090
Coniferous Woodland	0.080	0.060	0.120	0.101
Arable and Horticulture	0.040	0.025	0.045	0.037
Improved Grassland	0.035	0.035	0.060	0.035
Fen, Marsh and Swamp	0.062	0.040	0.120	0.058
Saltwater and Freshwater	0.025	0.020	0.040	0.033
Supralittoral and Littoral	0.020	0.010	0.025	0.018
Saltmarsh	0.075	0.060	0.120	0.071
Urban	0.025	0.020	0.040	0.033
Suburban	0.030	0.020	0.045	0.033

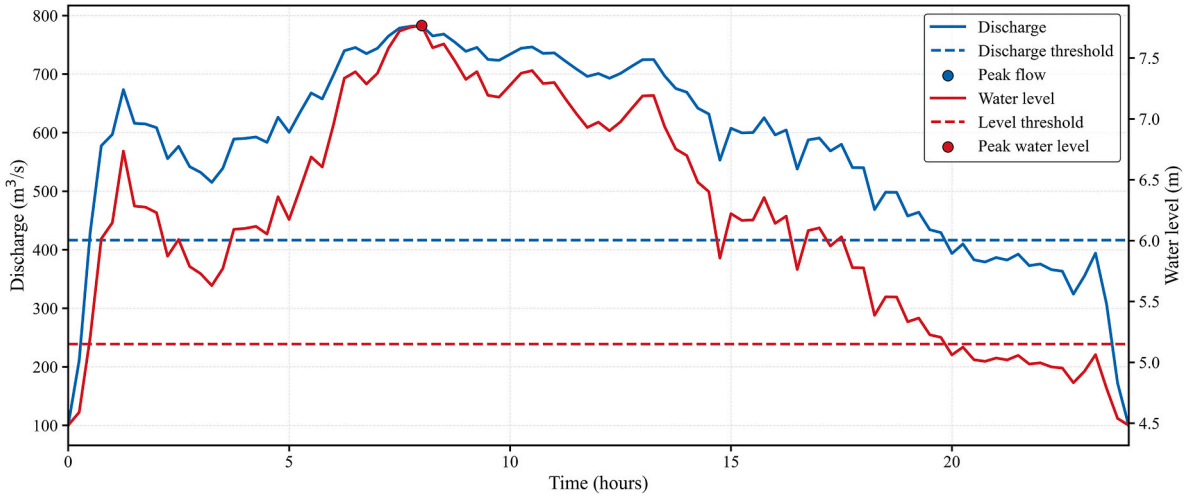


Fig. 6. Discharge and water level at Kingston Station for flood events occurred in 100-year flood.

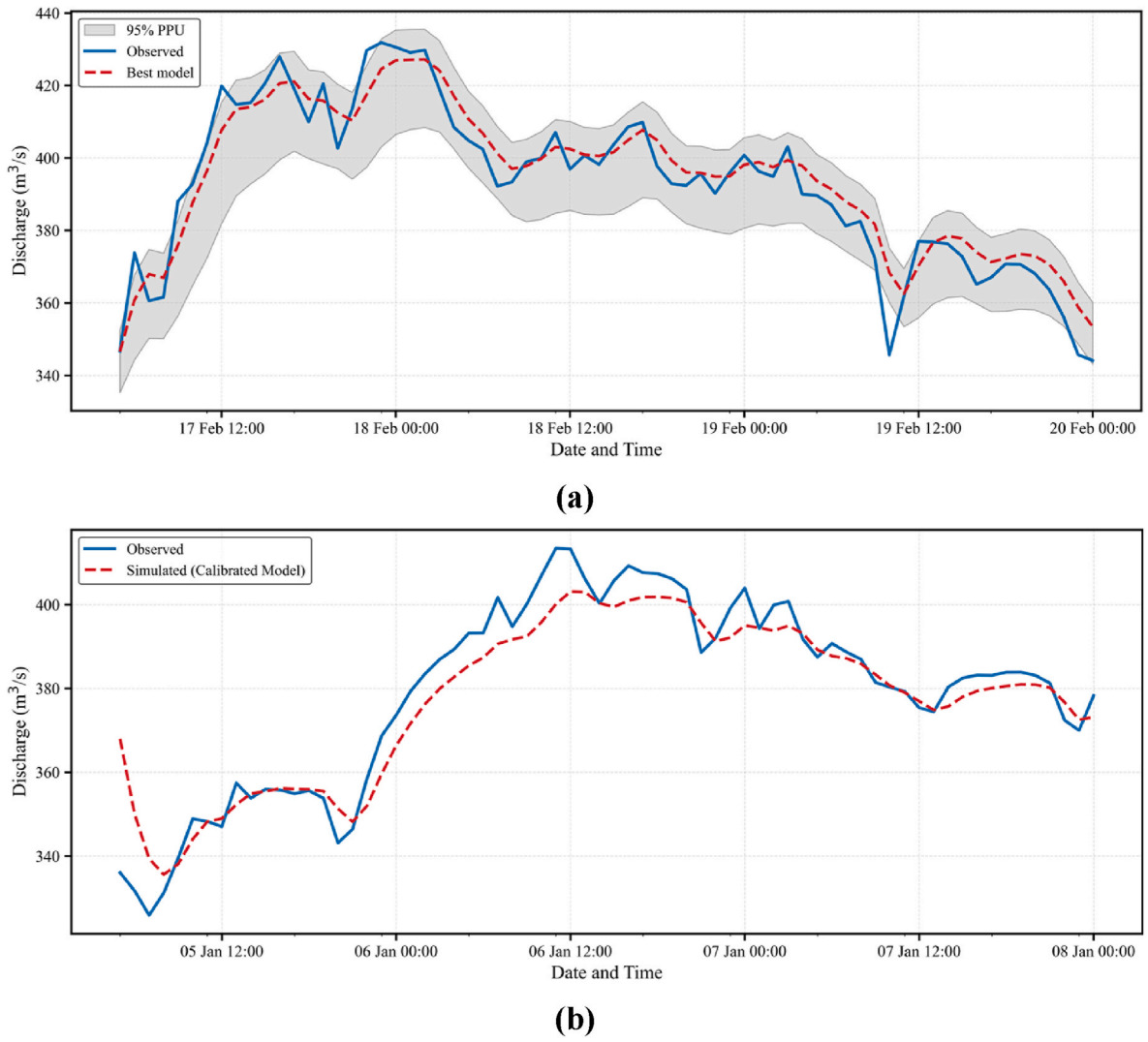


Fig. 7. Observed vs Simulated discharge at Kingston Station for (a) calibration (flood event in 2020) and (b) validation (flood event in 2024).

(Fig. 9c and d) show a more spatially dispersed distribution of travelling agents and comparatively fewer failed trips due to lower and more flexible travel demand. The dynamic evolution of road closures and changes in agent status throughout the simulation period for both weekday and weekend scenarios can be more clearly observed in Supplementary Video 1 and Supplementary Video 2, respectively, as described in Appendix D.

Supplementary data related to this article can be found online at https://doi.org/10.1016/j.envsoft.2026.107221

These findings provide practical insights for decision-makers by identifying spatial vulnerability hotspots for commuters during flood events. Across both scenarios, the results show a higher concentration of failed trips in the eastern and northern parts of the study area, highlighting these regions as critical zones for flood risk management. Based on this evidence, local authorities can prioritise these corridors in flood mitigation strategies, such as strengthening riverbank defence systems and incorporating these areas into early warning and traffic management plans to reduce mobility disruption during flood events. In particular, highly vulnerable road segments such as Hampton Court Road bridge and Sopwith Way shown in Fig. 8, should be prioritised, as disruption of these critical corridors can result in a significant increase in failed trips illustrated in Fig. 9a and b.

As shown in Fig. 10, the weekday and weekend results demonstrate a clear temporal interaction between road closures and agent mobility states. Road closures are dynamically updated at each time step based on the 100-year flood (shown in Fig. 6b). On weekdays (Fig. 10a), road closures increase gradually from early morning, reaching a peak of 8.5-9% between 15:00 and 18:30, which coincides with the highest disruption period in the transport network shown in Fig. 9b. During this interval, the number of travelling agents peaks at 21,000, while failed trips rise significantly to 36,720 (51% of total agents), indicating severe mobility disruption during the weekday commuter peak. As road closures decline after 20:00, the number of travelling agents decreases rapidly, and idle agents dominate overnight, reflecting reduced travel demand.

In contrast, Fig. 10b (weekend) shows that the number of travelling agents is lower under the same flood event and road-closure conditions. However, the number of failed trips remains high in the afternoon, reaching 32,400 (45% of total agents) because of the high number of road closures. In both time windows, the number of failed trips decreases as the roads gradually get opened. In this way, agents who were previously unable to identify a feasible route can resume travel once accessible road connections become available.

These results indicate that the highest level of mobility disruption occurs during the weekday afternoon peak (15:00-18:30) when road closures reach the highest level and failed trips increase, suggesting that this period should be prioritised for flood risk intervention. Local authorities can use this information to implement early warning systems,

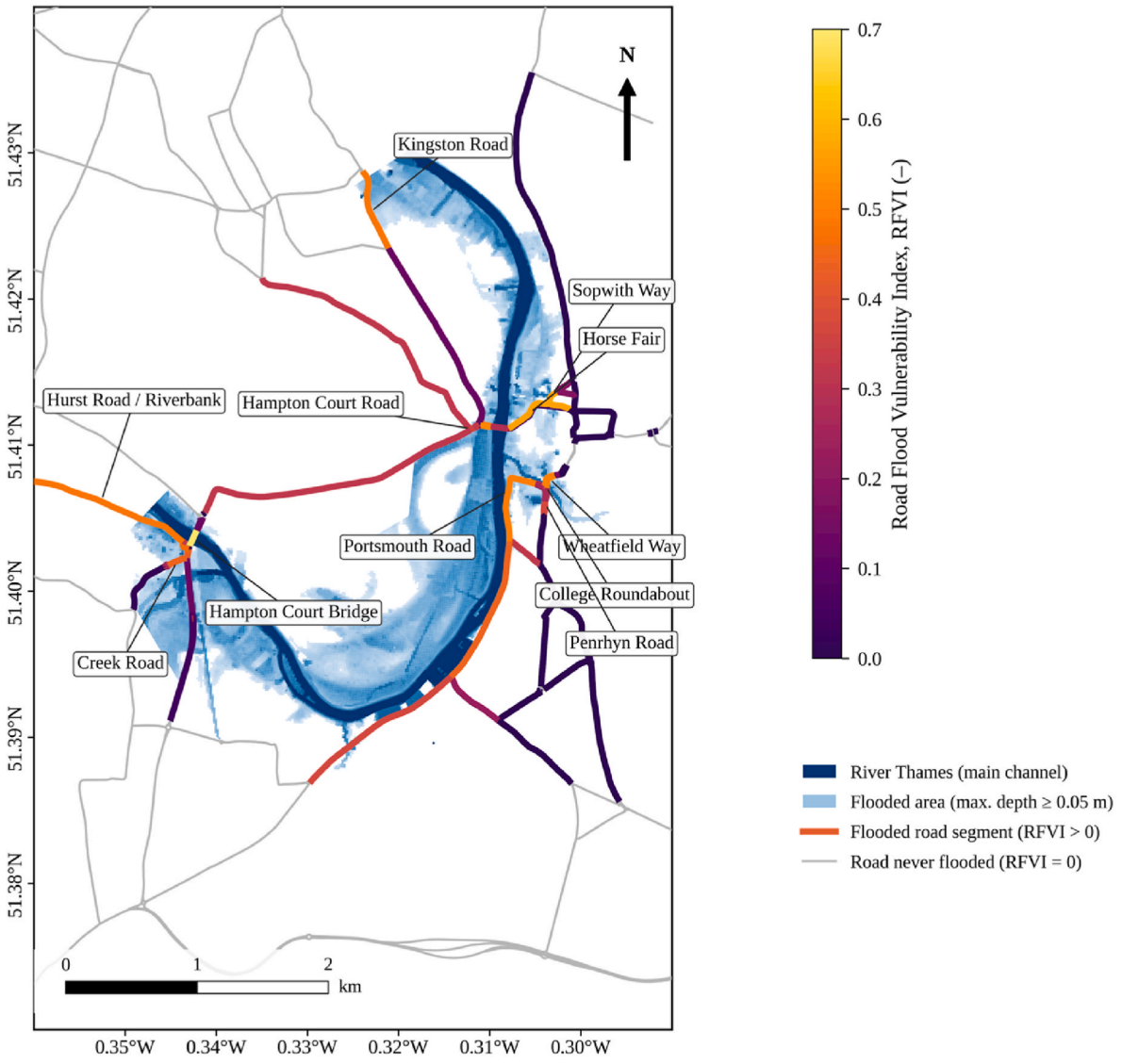


Fig. 8. Road flood vulnerability index under the 100-year flood scenario.

pre-emptive traffic diversions, and temporary closure management on vulnerable corridors before peak hours, thereby reducing failed trips and maintaining network functionality during flood events.

Flood impact assessment was further evaluated on demographic attributes through the relative risk index (RRI) to examine the impact on different age, employment-status, and travel-mode groups. The weekday and weekend RRI heatmap analyses shown in Figs. 11 and 12 reveal clear temporal and demographic disparities in flood exposure across the daily mobility cycle. The analyses are presented up to 2:00, as no significant travel activities occur beyond this period. In the weekday scenario (Fig. 11a), exposure is strongly influenced by structured commuting patterns, with adults consistently exhibiting moderate-to-high RRI values, generally ranging between approximately 0.8 and 1.8 throughout most of the daily mobility cycle. Although seniors experience the highest peak exposure levels, with RRI values frequently reaching 2-2.5 during midday periods, their exposure is more temporally concentrated. In contrast, adults remain continuously exposed across both morning and evening commuting periods, indicating more persistent flood-related mobility risk throughout the day. Children generally exhibit lower-to-moderate exposure levels, with intermittent peaks ranging between approximately 1 and 1.8 during active travel periods. The employment-based analysis (Fig. 11b) indicates that unemployed individuals experience the highest weekday exposure, with RRI values frequently exceeding 2, whereas employed individuals generally maintain moderate exposure levels between 1 and 2. Travel-mode analysis (Fig. 11c) further shows that cyclists and walkers often exceed RRI values of 2, while drivers and PTP typically range from 1 to 1.9, depending on the time of day.

In contrast, the weekend patterns, shown in Fig. 12, are more temporally distributed and less dominated by distinct peak periods. Based on Fig. 12a, children maintain high risk levels, peaking between 1.5 and 2.5, while adults and seniors experience localised peaks during recreational activity periods. The employment analysis (Fig. 12b) again highlights higher exposure for unemployed individuals, with peak RPI values approaching 2-2.5, while employed and student groups generally remain within 0.5-1.25. The result for the employment status analysis shown in Fig. 12c indicates that the Drivers and PTP groups frequently exhibit the highest weekend RRI values (around 1.5-2), reflecting increased recreational and local mobility.

The results indicate that the highest risk occurs during midday on weekdays and weekends, with the road closure reaching 9% (as shown in Fig. 10a–b). However, there are some high-risk times early in the morning, when people start their daily activities, and late at night, when people try to come home. The results suggest that targeted interventions,

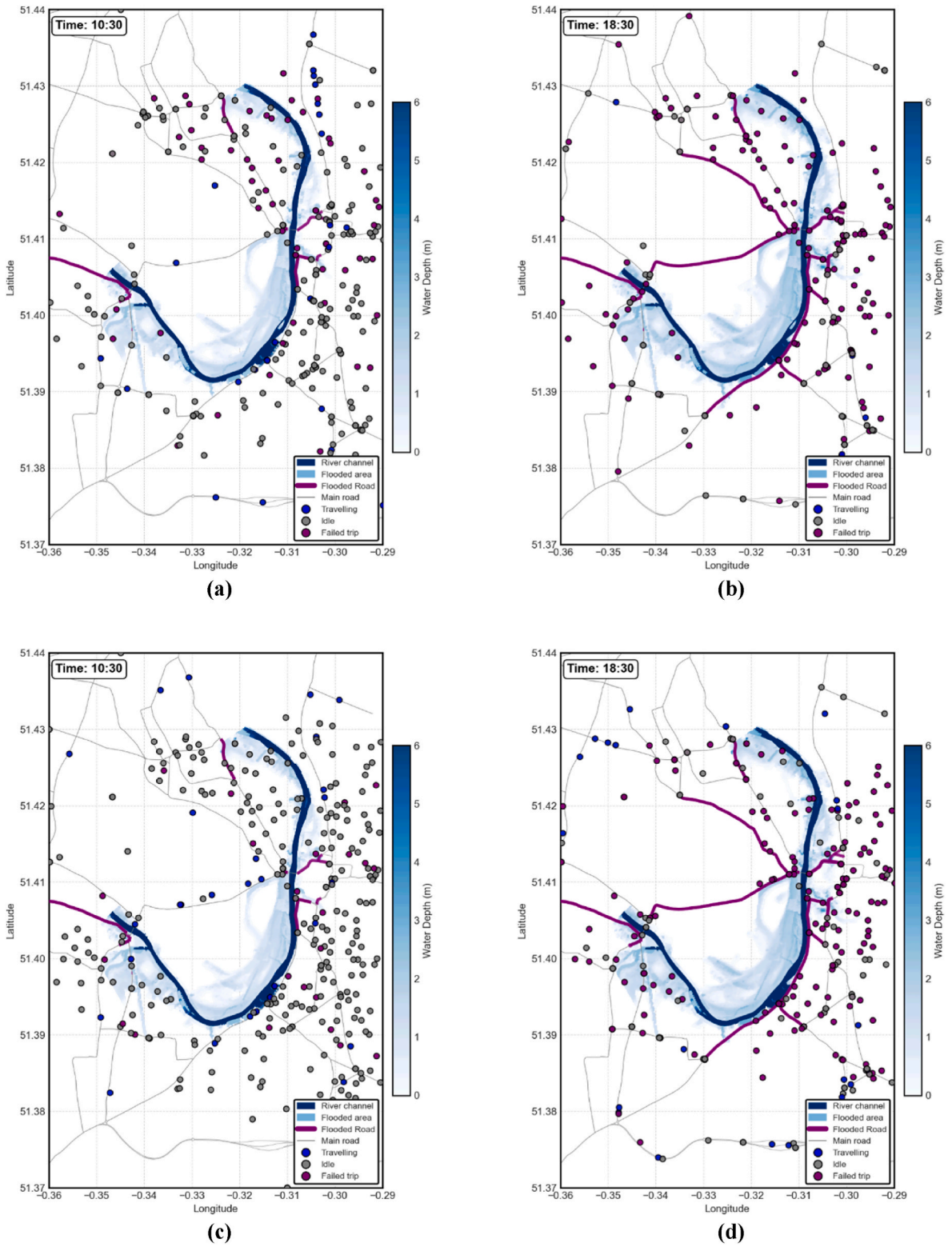


Fig. 9. Flooded roads and behaviour of agents over the 100-year flood scenario at (a) weekday 10:30, (b) weekday 18:30, (c) weekend 10:30, and (d) weekend 18:30. Selected snapshots were extracted from Supplementary Video 1 (weekday scenario) and Supplementary Video 2 (weekend scenario), described in Appendix D.

for specific groups such as the unemployed in both time windows or the senior group on weekdays, could significantly reduce mobility-related flood risk. For example, authorities can prioritise early warning systems and temporary traffic management measures during high-risk periods, particularly weekday afternoon travel windows when RRI values exceed 2-2.5 for several groups.

Vulnerable hotspots in flood risk assessment can be detected by integrating dynamic flood inundation maps with high-risk vulnerable agent distributions. Fig. 13 illustrates the spatio-temporal distribution of agents experiencing either high risk (RPI $>$ 0.8 for weekdays and RPI $>$ 0.7 for weekends) or direct exposure to hazardous flood depths (water depth $\geq$ 0.3 m) across different age groups and travel modes. Fig. 13a–b

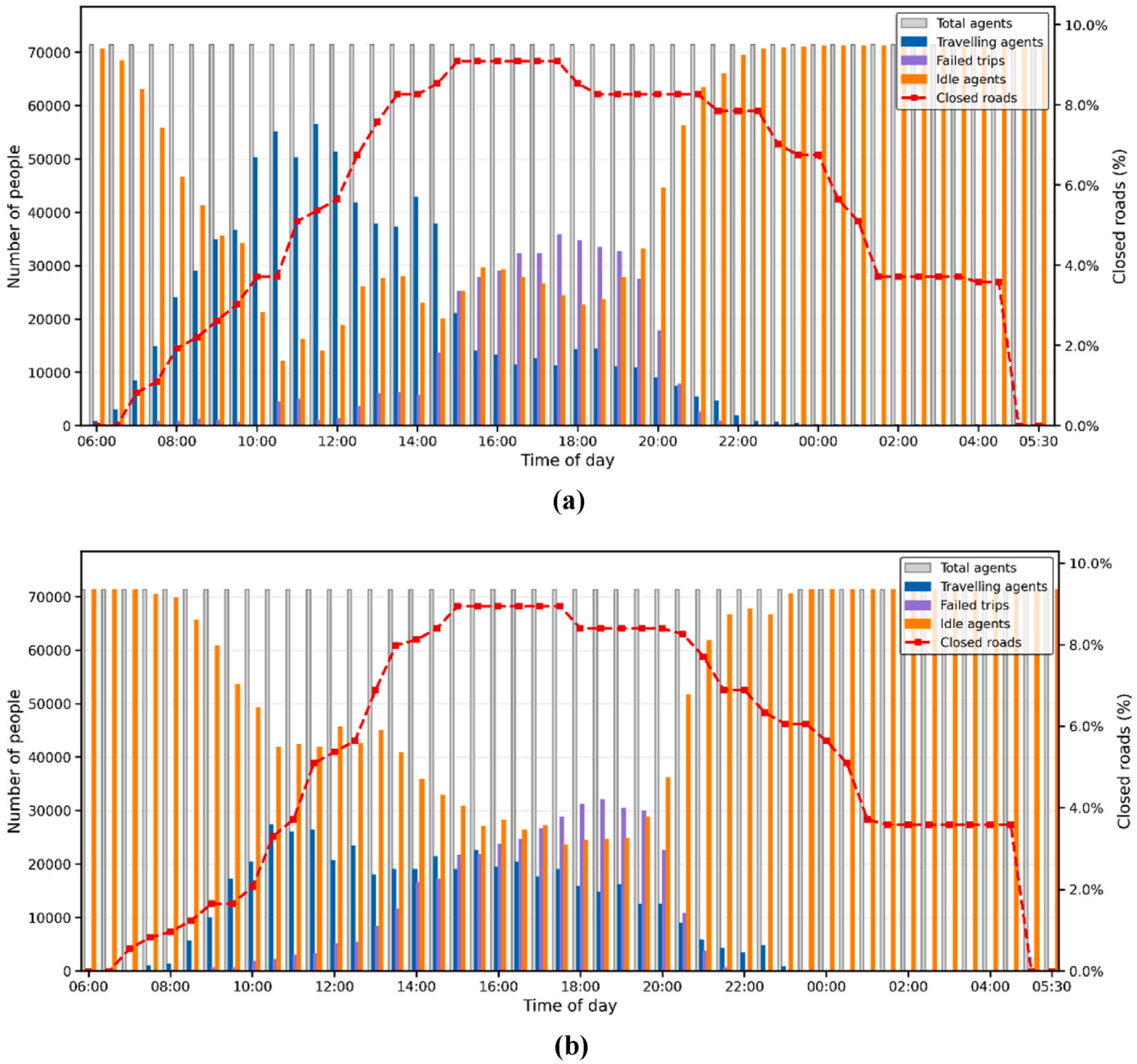


Fig. 10. Failed trip and the number of travelling agents for (a) weekday and (b) weekend.

represent weekday conditions at 10:30 and 18:30, while Fig. 13c–d correspond to the weekend scenarios at the same time intervals, respectively.

During the weekday morning period (Fig. 13a), vulnerable agents are predominantly located along river-adjacent transport corridors and bridge access points, where floodwater begins to encroach on key commuter routes. Adults using walking and driving modes appear most frequently near the floodplain boundaries, indicating higher exposure along daily travel paths. By the evening period (Fig. 13b), the spatial concentration of high-risk agents increases around flooded corridors and major crossing routes as return-home trips occur, with several seniors and children observed closer to deeper flood zones, suggesting limited mobility and fewer alternative route options. In contrast, the weekend scenarios shown in Fig. 13c–d displays a more spatially dispersed pattern of high-risk agents across the network. Like the weekday scenarios, vulnerable agents in the weekend scenarios remain distributed near flooded transport links, indicating that local travel activities continue to expose individuals to flood-related mobility risk under disrupted network conditions. Adults again appear to be the most exposed demographic group to flooding.

The results of dynamic vulnerable agent mapping highlighted that although high RPI values can lead to cancellation of non-essential trips like shopping and leisure related travel, still adults followed by senior and children's groups can be at risk during the peak travel time which should therefore be considered in flood risk management and emergency planning strategies.

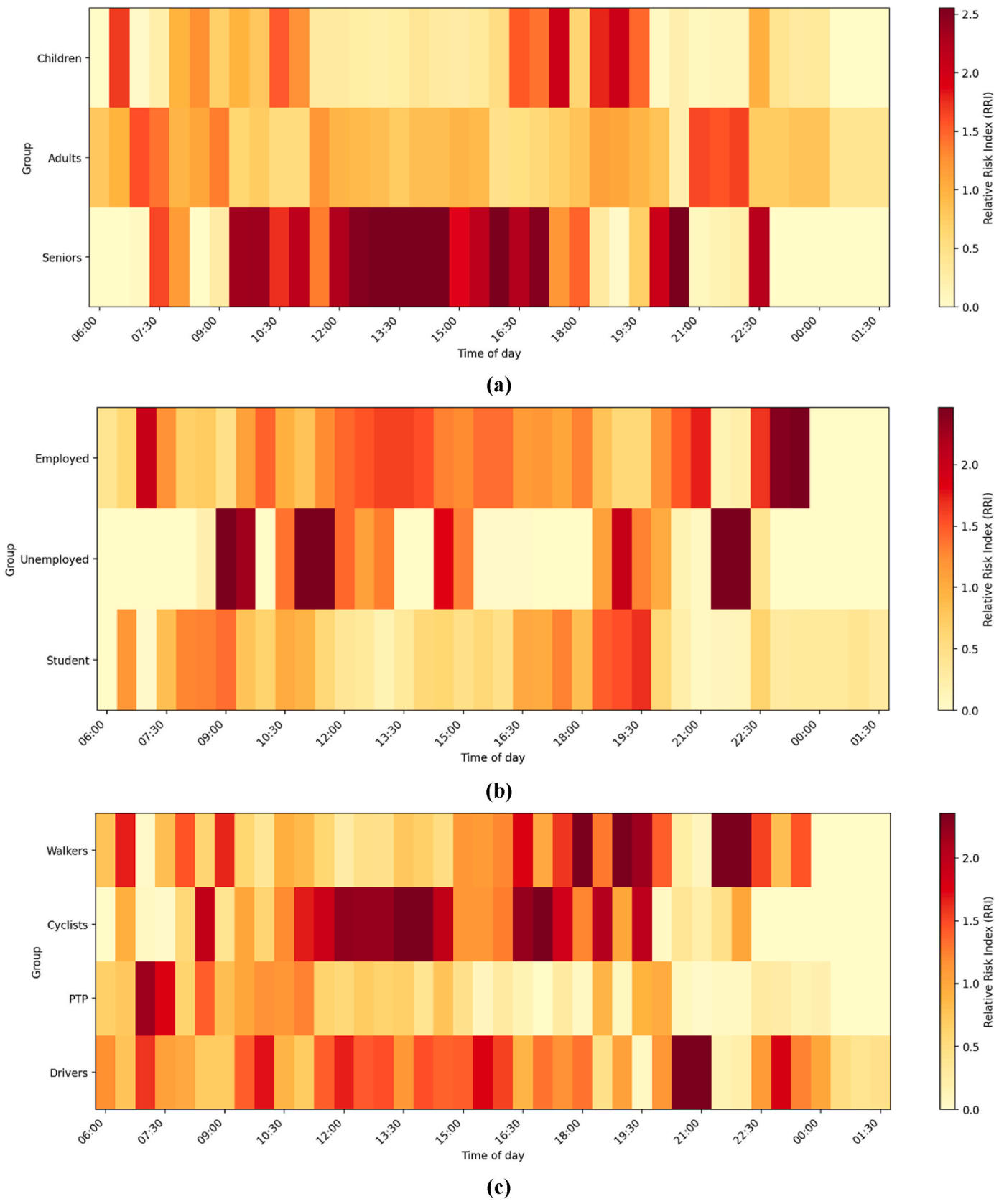


Fig. 11. Relative risk index by (a) age, (b) employment status, and (c) travel mode for weekday.

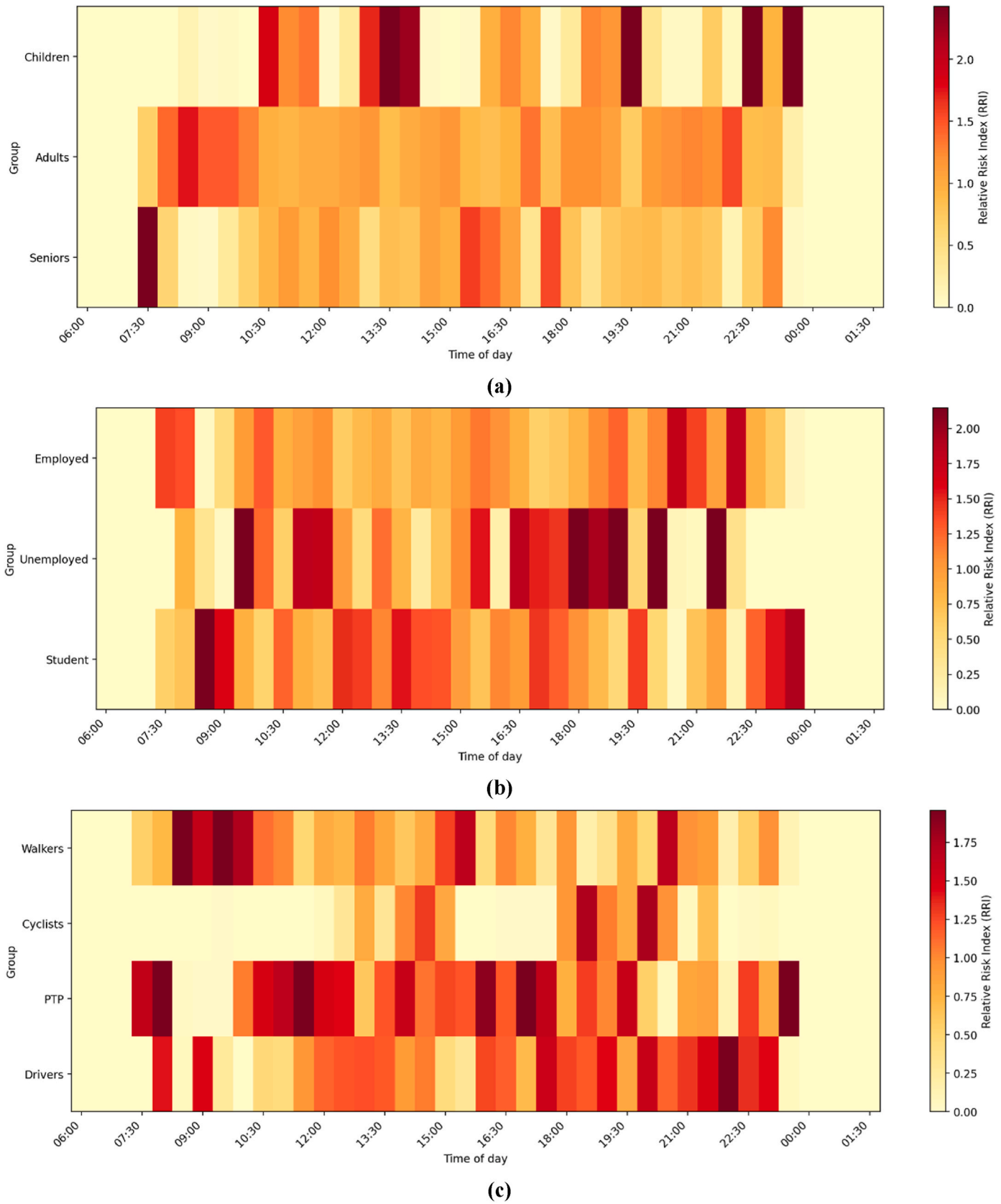


Fig. 12. Relative risk index by (a) age, (b) employment status, and (c) travel mode for the weekend.

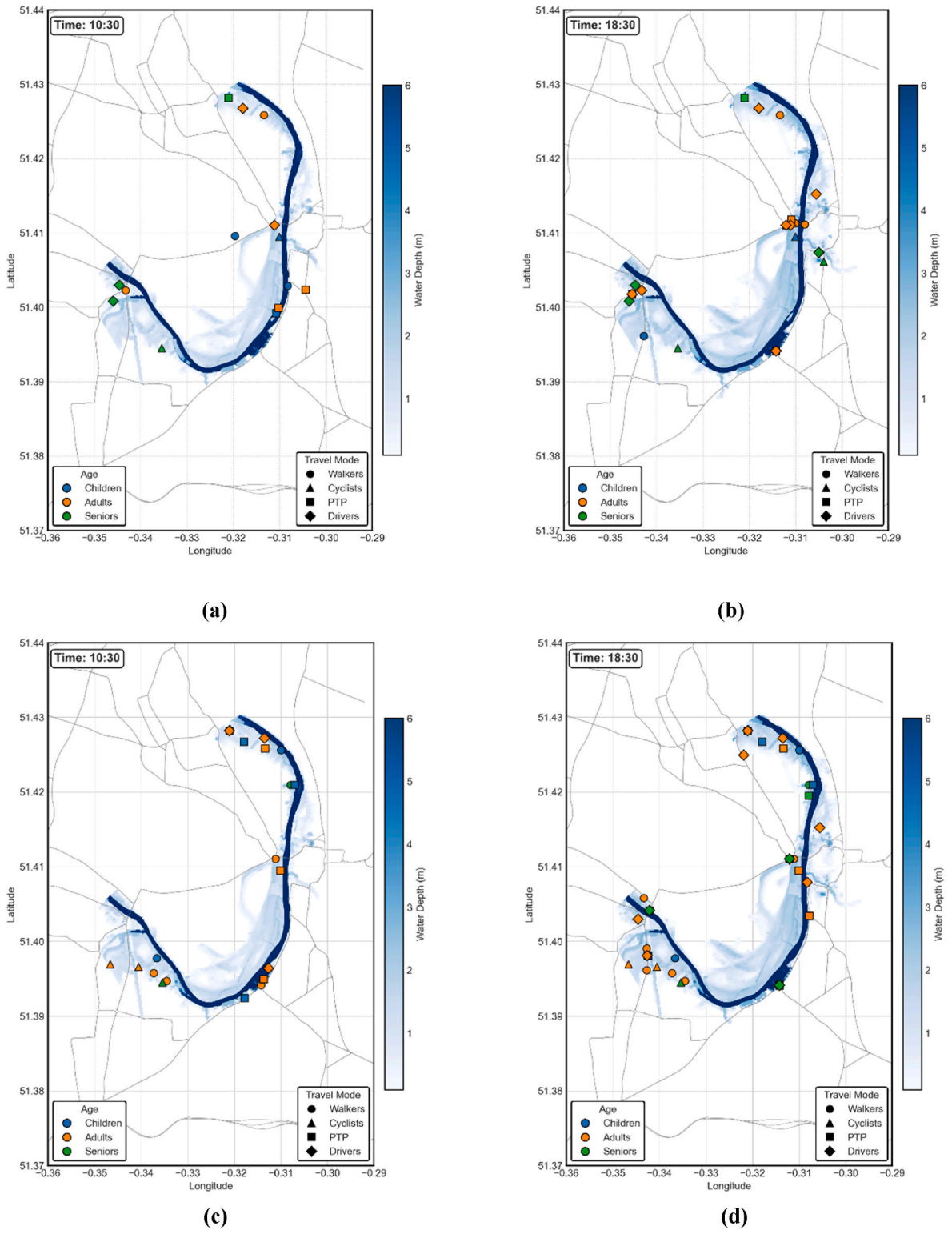


Fig. 13. Location of agents with high RPI under 100-year flood scenario (RPI> 0.8 for weekdays and RPI>0.7 for weekends) or water depth> 0.3m for different age and travel modes on weekdays at (a) 10:30, (b) 18:30, and at weekends at (c) 10:30, (d) 18:30.

3.4. Sensitivity and uncertainty of the hydrodynamic and behavioural models

3.4.1. Propagation of hydrodynamic uncertainty into the coupled impact assessment

The results in Section 3.2/3.3 are based on a single reference configuration. Their robustness was assessed by (i) propagating 18 behavioural SUFI-2 parameters set through the coupled simulation, (ii) varying the road-closure threshold between 0.20 and 0.40 m.

For propagation of SUFI-2 parameter sets, From the 60 parameter sets sampled in the three SUFI-2 iterations of the 2020 calibration, 18 behavioural sets were selected: all unique sets with $R^2 \geq 0.80$ for discharge at Kingston. Across the ensemble, the peak proportion of closed roads ranged from 8.3% to 9.9% (60-72 of the 726-road links;

Fig. 14 (a)). Peak failed trips ranged from 49.6% to 52.8% on the weekday as shown in Fig. 14 (b). The road links identified as most vulnerable in Section 3.3 closed in every ensemble member, so their ranking is preserved.

Regarding the sensitivity to the closure threshold, the coupled simulation was repeated with closure thresholds of 0.20, 0.25, 0.30, 0.35 and 0.40 m, with all other parameters fixed. Over this range, the peak proportion of closed roads varied from 8.3% to 9.4% (Fig. 15), and weekday failed trips from 50.8% to 52.7% (Fig. 16).

3.4.2. *Sensitivity analysis of mobility impacts to flood onset time*

The reference scenario assumes a fixed onset time of the 100-year hydrograph. In reality, onset is uncertain and may occur at any time of day, and the same hydrograph can lead to different mobility and exposure outcomes depending on how it overlaps with daily travel demand. In a risk-oriented application, onset time can be treated as a random variable by simulating a set of onset times and aggregating the results as probability-weighted expected values, envelopes or exceedance-probability curves. Simulations with onsets shifted by 0, 6 and 12 h (Appendix E, Figure E) showed that peak weekday failed trips ranged from 34.8% to 52.8%, with an onset-averaged value of 46.2%. The impact was smallest when the maximum road closure fell in the late evening (+6 h) and largest when roads remained closed into the evening travel peak (reference and +12 h). In all cases, failed trips peaked during the evening travel period (16:30-18:30), indicating that the overlap between persistent road closures and peak travel demand, rather than

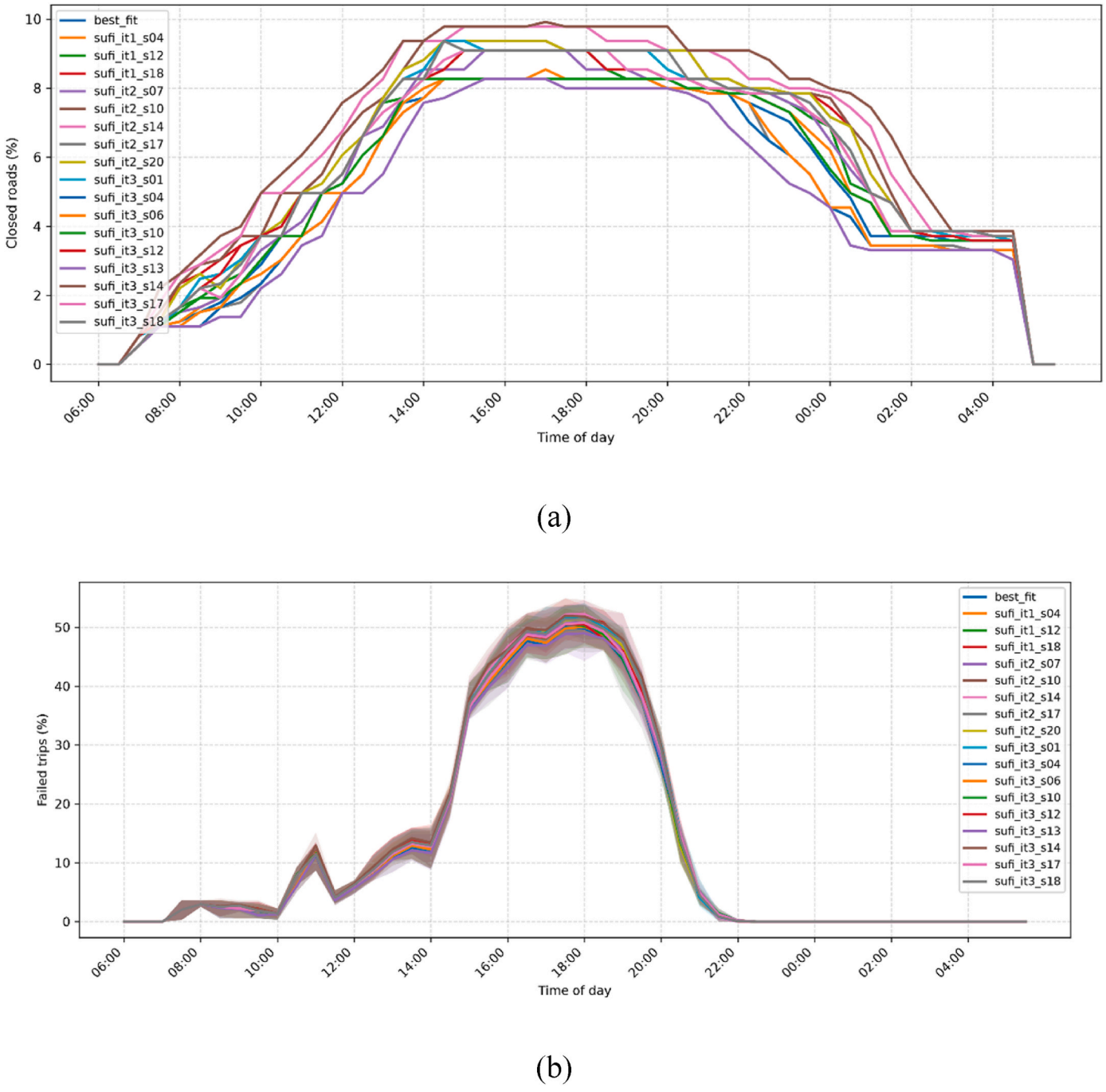


Fig. 14. Proportion of closed roads (a) and failed trips (b) in 18 behavioural sets for 100-year flood (the behavioural sets were sampled from the 2020 calibrated model).

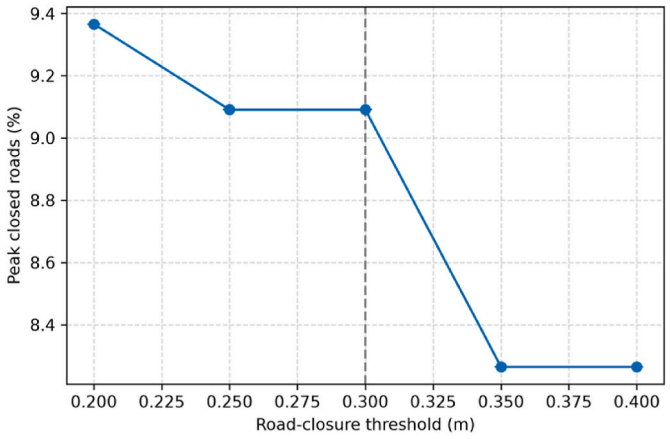


Fig. 15. Proportion of peak-closed roads for various road-closure thresholds.

the timing of the hydraulic peak alone, controls the mobility impact.

3.4.3. Sensitivity analysis of behavioural and social parameters

Three scenarios were implemented by varying λ within the RPI update rule. The Individualist scenario (λ = 1) represents agents who rely solely on personal environmental cues and completely disregard social signals. The Collectivist scenario (λ = 0) models' agents whose RPI is determined entirely by the average priority within their social neighbourhood, reflecting strong peer-driven behavioural contagion. The Balanced scenario (λ = 0.5) assigns equal weight to individual risk and social influence, resulting in an intermediate balance between self-driven and socially reinforced responses.

The RPI distribution dynamics (Fig. 17) highlight how different strengths of social influence (λ) shape collective risk priority throughout the day. In each violin chart on this figure, the dashed horizontal lines denote the median RPI and the interquartile range (25th-75th percentiles), enabling direct comparison of both central tendency and dispersion.

At 08:30, all three scenarios exhibit similar central tendencies, reflecting early-stage uncertainty where agents rely primarily on their own limited environmental cues. However, the distribution spread varies: the Individualist scenario (λ = 1.0, blue) shows the most well dispersion, indicating highly heterogeneous priorities as agents respond independently to local flood conditions. The Balanced scenario (λ = 0.5, orange) shows a narrower distribution with a slightly higher median RPI, demonstrating that moderate social influence enables risk signals to propagate without completely overriding personal cues. In contrast, the Collectivist scenario (λ = 0.0, green) produces the most concentrated distribution, as substantial social conformity drives agents toward a shared, group-averaged priority.

By 17:30, the Individualist population continues to exhibit the most significant variability, with some agents registering high risk while others remain comparatively unaware. The Balanced population maintains a stable, moderately elevated RPI with reduced dispersion, indicating effective but not overpowering social contagion. The Collectivist population again converges toward a tightly clustered distribution around a mid-range RPI, reflecting rapid consensus formation driven by peer influence. Together, these dynamics show that moderate social influence (λ = 0.5) produces the most coherent and responsive population-level awareness. At the same time, both extremes, pure individualism and pure collectivism, lead to either fragmented or overly homogenised priorities. The results highlight that flood warning strategies should combine official communications with mechanisms that support peer-to-peer information exchange, such as community networks and trusted local intermediaries.

It should be mentioned that the Watts-Strogatz small-world model was implemented with k = 4 and p = 0.2 to represent realistic patterns of social interaction during flood events. Setting k = 4 implies that each agent is directly influenced by a limited number of close social contacts, reflecting typical neighbourhood- or peer-based communication rather than unrealistically dense social connectivity (Watts and Strogatz, 1998). The rewiring probability with p = 0.2, the average path length is already short while about half of the lattice clustering is retained, so the network represents both local ties and long-range contacts (Barrat and Weigt, 2000). As a result, the simulated network exhibits clear small-world characteristics, where localised patterns of risk perception coexist with rapid city-wide diffusion triggered by social shortcuts.

Varying the demographic increment between 0 and 0.3 changed peak weekday failed trips by only −0.84 to +0.78 percentage points (Fig. 18), well within the variability between random seeds. For the weights of flood depth and official warning, which in the reference case give greater weight to locally experienced depth (α = 0.7, β = 0.3), setting α/β to 0.5/0.5 and 0.9/0.1 changed peak failed trips by +0.90 and −0.17 percentage points. A stronger weight on the warning raises the RPI of all agents while the warning is active, whereas a weaker weight confines high RPI values to agents in flooded locations. Increasing the number of social neighbours from K = 4 to 6 and 10

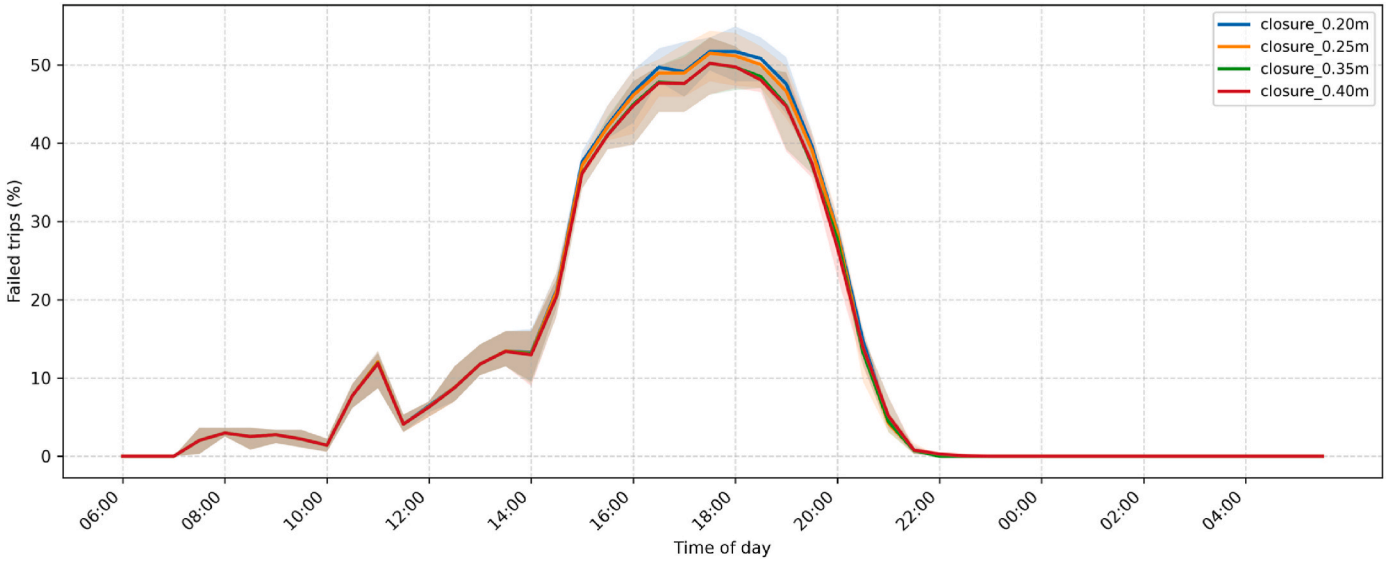


Fig. 16. Proportion of failed trips for different road closure thresholds.

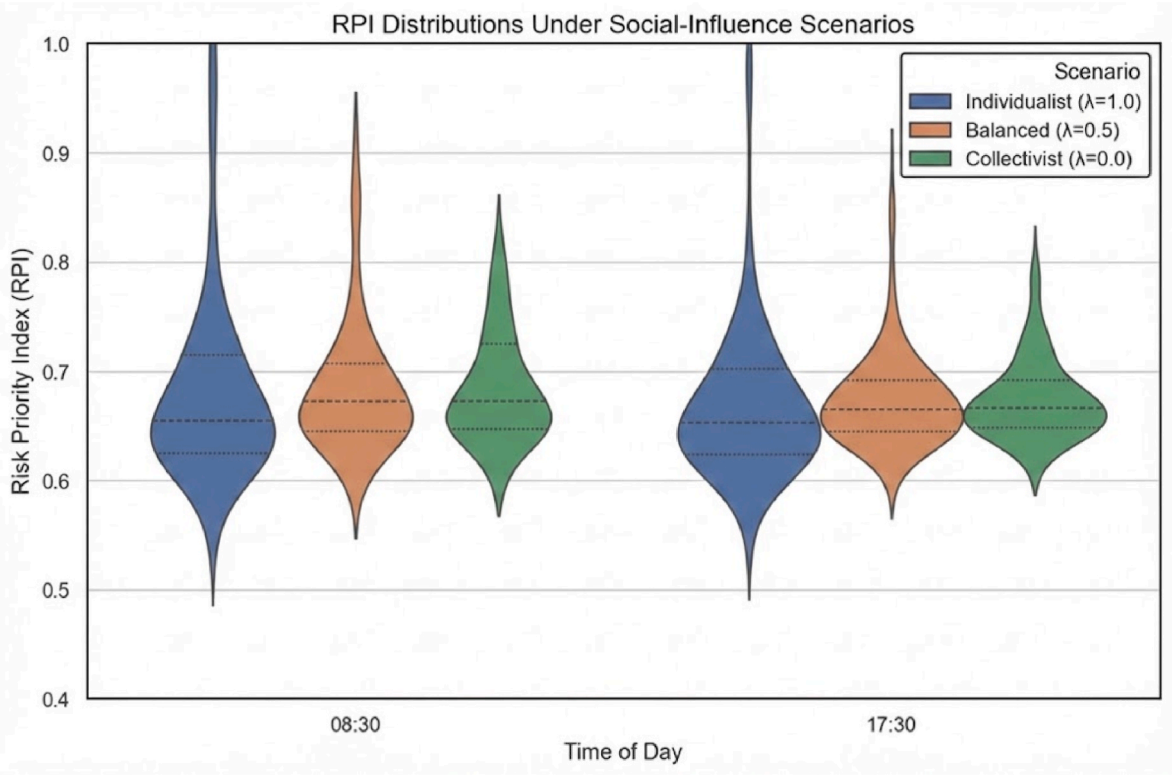


Fig. 17. RPI distribution under the various social scenarios (individualist, balanced, and collectivist).

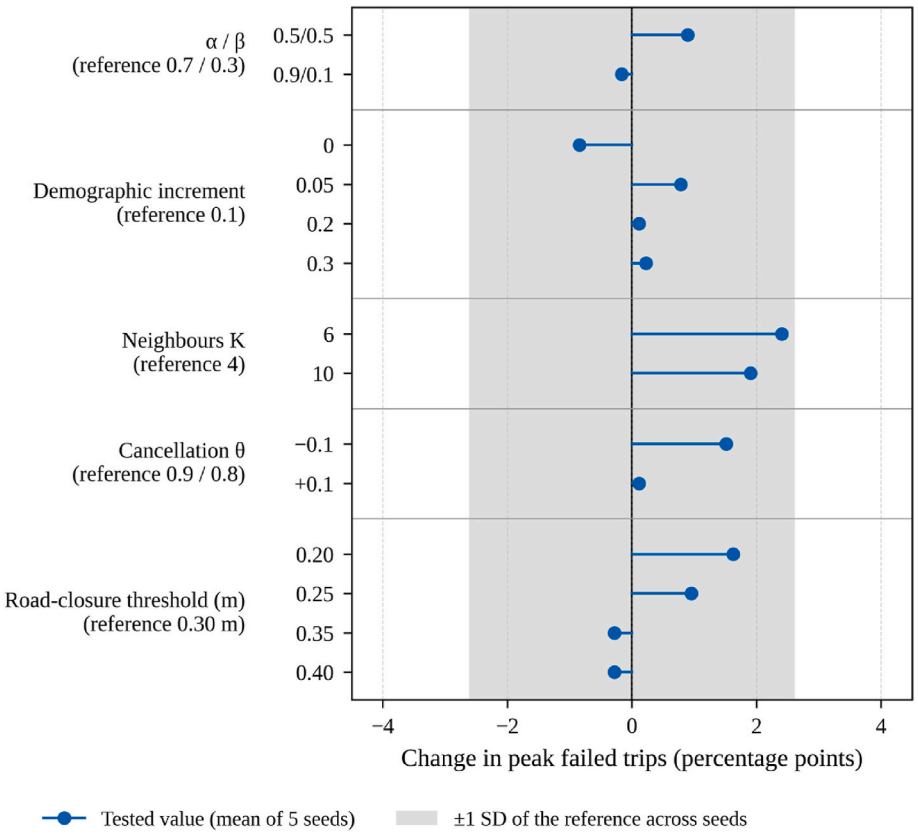


Fig. 18. Sensitivity of peak weekday failed trips to the behavioural parameters and the road-closure threshold, expressed as the change from the reference configuration in percentage points. Each point is the mean of five random seeds; the grey band shows ±1 standard deviation of the reference across seeds.

produced the largest changes in peak failed trips (+2.41 and + 1.90 percentage points), which still remain within one standard deviation of

the reference across seeds (grey band in Fig. 18). The trip-cancellation thresholds ($\theta = 0.9$ for commuting and 0.8 for other trips) were varied by ± 0.1; with $+0.1$ the commuting threshold becomes 1.0, so commuting trips are never cancelled voluntarily. These changes altered peak failed trips by only $+1.51$ and $+ 0.11$ percentage points. Finally, varying the road-closure threshold between 0.20 and 0.40 m (reference 0.30 m; Pregnolato et al., 2017) changed the peak share of closed roads from 9.09% to between 8.26% and 9.37%. Peak failed trips then ranged from 50.76% to 52.66% (-0.28 to $+1.62$ percentage points).

4. Conclusions

An integrated modelling framework was developed that couples a calibrated hydrodynamic flood model with a dynamic agent-based model to assess the impacts of urban flooding on transportation systems, traveller behaviour, and demographic vulnerability. The hydrodynamic model demonstrated strong calibration and validation performance using historical flood events at Kingston Station through the SUFI-2 uncertainty-based calibration procedure, achieving R^2 values of 0.91 and 0.89 for the calibration and validation events, respectively, thereby ensuring reliable flood simulations for mobility-impact analysis.

Results indicate that flood-induced road closures affected 9% of the transport network, causing substantial mobility disruption, with approximately 51% of trips failing during weekdays and 45% during weekends. Spatial analysis identified critical vulnerability hotspots along the Thames corridor and major bridge access routes, particularly Hampton Court Road Bridge and Sopwith Way, which exhibited the highest RFVI values of 0.69 and 0.57, respectively. The results further revealed clear temporal and demographic disparities in flood exposure across population groups and travel modes. Adults remained continuously exposed during weekday morning and evening commuting periods, while seniors exhibited the highest RRI values during midday and late-night periods. Employment-based analysis showed that unemployed individuals experienced the highest exposure levels, frequently exceeding RRI values of 2-2.5. In addition, active travel modes such as walking and driving demonstrated the highest exposure levels during peak weekday travel periods.

These results indicate that mobility disruption during floods is influenced not only by hydrodynamic severity but also by travel demand patterns and socio-demographic characteristics. Consequently, the framework offers a practical tool for evaluating urban flood resilience and supporting evidence-based decision-making in flood risk management. For example, the framework can support emergency response prioritisation for critical infrastructure and densely populated regions by identifying highly vulnerable corridors during extreme flood events. In addition, it can assist urban planners and local authorities in developing flood-resilient transportation and evacuation strategies by evaluating the impacts of dynamic road closures and alternative routing scenarios under different flood conditions.

Future research should enhance the framework by incorporating the validation of the agent-based model through survey-based investigations of demographic attributes and behavioural responses, thereby improving the realism and reliability of the behavioural simulation component. Moreover, additional heterogeneity factors such as previous flood experience, household composition (e.g., presence of children or elderly dependents), health conditions, socio-economic status, and accessibility to transportation resources could be integrated into the agent-based model to improve the realism and accuracy of behavioural simulations. The RPI and the road-closure criterion are based on water depth only. Although this is consistent with depth-based flood warnings and vehicle disruption criteria, and with the slow-rising fluvial flooding of the study area, it may underestimate the hazard to pedestrians and cyclists where flow velocities are higher. Future work should therefore incorporate higher velocity into the RPI and into mode-specific closure and exposure criteria.

Future developments should also validate the spatial performance of the hydrodynamic model against observed data, such as high-water marks, flood photographs or recorded road closures, when such data become available. Finally, integrating real-time flood forecasting with the ABM framework could support adaptive and dynamic response strategies during flood events, enabling more effective evacuation planning and emergency management.

CRediT authorship contribution statement

Saeid Najjar-Ghabel: Writing – review & editing, Writing – original draft, Visualization, Validation, Methodology, Investigation, Formal analysis, Data curation, Conceptualization. **Farzad Piadeh:** Writing – review & editing, Visualization, Supervision, Methodology, Formal analysis, Data curation, Conceptualization. **Kourosh Behzadian:** Writing – review & editing, Supervision, Methodology, Formal analysis, Data curation, Conceptualization. **Atiyeh Ardakanian:** Writing – review & editing, Supervision, Methodology, Conceptualization.

Declaration of generative AI in scientific writing

During the preparation of this work the authors used ChatGPT to improve readability and language of the text. After using this tool/service, the authors reviewed and edited the content as needed and take full responsibility for the content of the publication.

Declaration of competing interest

The authors declare that they have no known competing financial interests or personal relationships that could have appeared to influence the work reported in this paper.

Acknowledgement

This work is supported by the PhD scholarship allocated to the first author. The authors wish to acknowledge the PhD Vice Chancellor Scholarship supported by the University of West London.

Appendix A. Supplementary data

Supplementary data to this article can be found online at https://doi.org/10.1016/j.envsoft.2026.107221.

Data availability

Datasets used in this study is available in the GitHub repository.

References

Abebe, Y.A., Ghorbani, A., Nikolic, I., Vojinovic, Z., Sanchez, A., 2019. A coupled flood-agent-institution modelling (CLAIM) framework for urban flood risk management. Environ. Model. Software 111, 483–492. https://doi.org/10.1016/j.envsoft.2018.10.015.

Addai, O.A., Soares, C.P., Dhawale, R.S., Schuster-Wallace, C.J., Spiteri, R.J., 2025. Flood-ABM: an agent-based model of differential flood effects on population groups and their decision-making processes. Int. J. Disaster Risk Reduct. 128, 105698. https://doi.org/10.1016/j.ijdrr.2025.105698.

Arrighi, C., Oumeraci, H., Castelli, F., 2017. Hydrodynamics of pedestrians' instability in floodwaters. Hydrol. Earth Syst. Sci. 21, 515–531. https://doi.org/10.5194/hess-21-515-2017.

Auld, J., Mohammadian, A., 2012. Activity planning processes in the Agent-based dynamic activity planning and travel scheduling (ADAPTS) model. Transp. Res. Part A Policy Pract. 46, 1386–1403. https://doi.org/10.1016/j.tra.2012.05.017.

Bakhtiari, V., Piadeh, F., Behzadian, K., Kapelan, Z., 2023. A critical review for the application of cutting-edge digital visualisation technologies for effective urban flood risk management. Sustain. Cities Soc. 99, 104958. https://doi.org/10.1016/j.scs.2023.104958.

Bakhtiari, V., Piadeh, F., Chen, A.S., Behzadian, K., 2024. Stakeholder analysis in the application of cutting-edge digital visualisation technologies for urban flood risk management: a critical review. Expert Syst. Appl. 236, 121426. https://doi.org/10.1016/j.eswa.2023.121426.

Barrat, A., Weigt, M., 2000. On the properties of small-world network models. Eur. Phys. J. B 13, 547–560. https://doi.org/10.1007/s100510050067.
Butters, O., Dawson, R.J., 2025. Flood evacuation in informal settlements: application of an agent-based model to kibera using open data. Urban Sci. 9, 12. https://doi.org/10.3390/urbansci9010012.
Cox, R.J., Shand, T.D., Blacka, M.J., 2010. AUSTRALIAN RAINFALL AND RUNOFF REVISION PROJECT 10: APPROPRIATE SAFETY CRITERIA FOR PEOPLE.
Crooks, A., Heppenstall, A., Malleson, N., Manley, E., 2021. Agent-based modeling and the city: a gallery of applications, 885–910. https://doi.org/10.1007/978-981-15-8983-6_46.
Dechter, R., Pearl, J., 1985. Generalized best-first search strategies and the optimality of A. J. ACM 32, 505–536. https://doi.org/10.1145/3828.3830.
El Bilali, A., Taleb, A., Boutahri, I., 2021. Application of HEC-RAS and HEC-LifeSim models for flood risk assessment. Journal of Applied Water Engineering and Research. https://doi.org/10.1080/23249676.2021.1908183, 9, 336–351.
Environment Agency, 2025. Hydrological data and river levels [WWW Document]. Retrieved from. https://environment.data.gov.uk/.
Hamilton, K., Demant, D., Peden, A.E., Hagger, M.S., 2020. A systematic review of human behaviour in and around floodwater. Int. J. Disaster Risk Reduct. 47, 101561. https://doi.org/10.1016/j.ijdrr.2020.101561.
Hart, P., Nilsson, N., Raphael, B., 1968. A formal basis for the heuristic determination of minimum cost paths. IEEE Trans. Syst. Sci. Cybern. 4, 100–107. https://doi.org/10.1109/TSSC.1968.300136.
Jenkins, K., Surminski, S., Hall, J., Crick, F., 2017. Assessing surface water flood risk and management strategies under future climate change: insights from an agent-based model. Sci. Total Environ. 595, 159–168. https://doi.org/10.1016/j.scitotenv.2017.03.242.
Jonkman, S.N., Curran, A., Bouwer, L.M., 2024. Floods have become less deadly: an analysis of global flood fatalities 1975–2022. Nat. Hazards 120, 6327–6342. https://doi.org/10.1007/s11069-024-06444-0.
Khoshkonesh, A., Nazari, R., Nikoo, M.R., Karimi, M., 2024. Enhancing flood risk assessment in urban areas by integrating hydrodynamic models and machine learning techniques. Sci. Total Environ. 952, 175859. https://doi.org/10.1016/j.scitotenv.2024.175859.
Kunreuther, H., Pauly, M., 2006. Rules rather than discretion: lessons from hurricane katrina. J. Risk Uncertain. 33, 101–116. https://doi.org/10.1007/s11166-006-0173-x.
Kvočka, D., Falconer, R.A., Bray, M., 2016. Flood hazard assessment for extreme flood events. Nat. Hazards 84, 1569–1599. https://doi.org/10.1007/s11069-016-2501-z.
Lazzarin, T., Chen, A.S., Viero, D.P., 2024. Beyond flood hazard. Mapping the loss probability of pedestrians to improve risk estimation and communication. Sci. Total Environ. 912, 168718. https://doi.org/10.1016/j.scitotenv.2023.168718.
Lazzarin, T., Viero, D.P., Molinari, D., Ballio, F., Defina, A., 2022. Flood damage functions based on a single physics- and data-based impact parameter that jointly accounts for water depth and velocity. J. Hydrol. (Amst) 607, 127485. https://doi.org/10.1016/j.jhydrol.2022.127485.
Lo, A.Y., 2013. The role of social norms in climate adaptation: mediating risk perception and flood insurance purchase. Glob. Environ. Change 23, 1249–1257. https://doi.org/10.1016/j.gloenvcha.2013.07.019.
Lumbroso, D., Davison, M., Wetton, M., 2023. Development of an agent-based model to improve emergency planning for floods and dam failures. J. Hydroinform. 25, 1610–1628. https://doi.org/10.2166/hydro.2023.194.
Lv, W., Deng, F., Wang, J., Han, Y., Yang, S., 2025. Large-scale real-time evacuation modeling during urban floods: a coupled agent-based multi-model framework. Simulat. Model. Pract. Theor. 140, 103075. https://doi.org/10.1016/j.simpat.2025.103075.
Masoumi, F., Najjar-Ghabel, S., Safarzadeh, A., Sadaghat, B., 2020. Automatic calibration of the groundwater simulation model with high parameter dimensionality using sequential uncertainty fitting approach. Water Sci. Technol. Water Supply 20, 3487–3501. https://doi.org/10.2166/ws.2020.241.
Masoumi, F., Najjar-Ghabel, S., Salimi, N., 2021. Automatic calibration of the two-dimensional hydrodynamic and water quality model using sequential uncertainty fitting approach. Environ. Monit. Assess. 193. https://doi.org/10.1007/s10661-020-08831-z.
Michaelis, T., Brandimarte, L., Mazzoleni, M., 2020. Capturing flood-risk dynamics with a coupled agent-based and hydraulic modelling framework. Hydrol. Sci. J. 65, 1458–1473. https://doi.org/10.1080/02626667.2020.1750617.
Nagel, K., Wolf, D.E., Wagner, P., Simon, P., 1998. Two-lane traffic rules for cellular automata: a systematic approach. Phys. Rev. E 58, 1425–1437. https://doi.org/10.1103/PhysRevE.58.1425.
Najjar Ghabel, S., Zarghami, M., Akhbari, M., Nadiri, A.A., 2019. Groundwater management in Ardabil plain using agent-based modeling. Iran-Water Resources Research 15, 1–16.
Nazemi, A.R., Dolatshahi, M., Kerachian, R., 2024. A decentralized multi-agent framework for urban flood management. Sustain. Cities Soc. 106, 105328. https://doi.org/10.1016/j.scs.2024.105328.
Office for National Statistics, 2021. Building and demographic data [WWW Document]. https://www.ons.gov.uk/.
OpenStreetMap, 2025. OpenStreetMap data [WWW Document]. Available at: https://www.openstreetmap.org.
Piadeh, F., Ahmadi, M., Behzadian, K., 2022a. A novel framework for planning policy and responsible stakeholders in industrial wastewater reuse projects: a case study in Iran. Water Policy 24, 1541–1558. https://doi.org/10.2166/wp.2022.078.
Piadeh, F., Behzadian, K., Alani, A.M., 2022b. A critical review of real-time modelling of flood forecasting in urban drainage systems. J. Hydrol. (Amst) 607, 127476. https://doi.org/10.1016/j.jhydrol.2022.127476.
Piadeh, F., Behzadian, K., Chen, A.S., Campos, L.C., Rizzuto, J.P., Kapelan, Z., 2023. Event-based decision support algorithm for real-time flood forecasting in urban drainage systems using machine learning modelling. Environ. Model. Software 167, 105772. https://doi.org/10.1016/j.envsoft.2023.105772.
Piadeh, Farzad, Bakhtiari, V., Piadeh, Farshad, 2026. Automated novel real-time framework for rainfall data imputation in flood early warning systems. Eng. Appl. Artif. Intell. 164, 113348. https://doi.org/10.1016/j.engappai.2025.113348.
Pregnolato, M., Ford, A., Wilkinson, S.M., Dawson, R.J., 2017. The impact of flooding on road transport: a depth-disruption function. Transp. Res. D Transp. Environ. 55, 67–81. https://doi.org/10.1016/j.trd.2017.06.020.
Qin, H., Liang, Q., Chen, H., De Silva, V., 2024. A high-performance coupled human and natural systems (CHANS) model for flood risk assessment and reduction. Water Resour. Res. 60. https://doi.org/10.1029/2023WR036269.
Shabanpour, R., Javanmardi, M., Fasihozaman, M., Miralinaghi, M., Mohammadian, A., 2018. Investigating the applicability of ADAPTS activity-based model in air quality analysis. Travel Behav. Soc. 12, 130–140. https://doi.org/10.1016/j.tbs.2017.02.004.
Solomatine, D.P., Ostfeld, A., 2008. Data-driven modelling: some past experiences and new approaches. J. Hydroinform. 10, 3–22. https://doi.org/10.2166/hydro.2008.015.
Templeton, A., Xie, H., Gwynne, S., Hunt, A., Thompson, P., Köster, G., 2024. Agent-based models of social behaviour and communication in evacuations: a systematic review. Saf. Sci. 176, 106520. https://doi.org/10.1016/j.ssci.2024.106520.
Transport for London, 2024. London Travel Demand Survey (LTDS) [WWW Document]. Available at: https://tfl.gov.uk/.
UK Centre for Ecology & Hydrology, 2025. Land cover map (LCM). Retrieved from. https://www.ceh.ac.uk/.
United Nations General Assembly (UNGA), 2016. Report of the open-ended Intergovernmental Expert Working Group on Indicators and Terminology Relating to Disaster Risk Reduction. New York.
Watts, D.J., Strogatz, S.H., 1998. Collective dynamics of 'small-world' networks. Nature 393, 440–442. https://doi.org/10.1038/30918.
Zhang, K., Shalehy, M.H., Ezaz, G.T., Chakraborty, A., Mohib, K.M., Liu, L., 2022. An integrated flood risk assessment approach based on coupled hydrological-hydraulic modeling and bottom-up hazard vulnerability analysis. Environ. Model. Software 148, 105279. https://doi.org/10.1016/j.envsoft.2021.105279.
Zhang, R., Liu, D., Du, E., Xiong, L., Chen, J., Chen, H., 2024. An agent-based model to simulate human responses to flash flood warnings for improving evacuation performance. J. Hydrol. (Amst) 628, 130452. https://doi.org/10.1016/j.jhydrol.2023.130452.
Zhuo, L., Han, D., 2020. Agent-based modelling and flood risk management: a compendious literature review. J. Hydrol. (Amst) 591, 125600. https://doi.org/10.1016/j.jhydrol.2020.125600.